LEHMAN, ADAM, M.A. Remote Sensing Analysis of Urban Heat Island Effects on Selected Impervious Surfaces in Western Guilford County, NC, 2022.
Directed by Drs Keith Debbage and Wenliang Li. 62 pgs.

This research paper aims to provide a quantifiable measurement of albedo and surface temperature of selected sites in the western part of Guilford County, NC, near the cities of Greensboro, High Point, and Kernersville, highlighting specific grey infrastructures (GREIs) for analysis and comparison. The purpose of this research paper is to provide evidence of which roofing technology or technique potentially contributes the least to the urban heat islands (UHIs) of this study area.

Based on the finding of this study, many of the rooftop materials performed as expected. In all cases, there was a positive correlation between Greensboro temperature and all of the roofs in this case study. This study suggests that the GREIs represented do demonstrate cooling potential and monitoring GREIs will continue to help ascertain the effectiveness of future construction materials for low-slope roofs as an effective way to help reduce urban temperatures or mitigate the effects of UHIs.

REMOTE SENSING ANALYSIS OF URBAN HEAT ISLAND EFFECTS ON SELECTED IMPERVIOUS SURFACES IN WESTERN GUILFORD COUNTY, NC, 2022

by

Adam Lehman

A Thesis

Submitted to

the Faculty of The Graduate School at

The University of North Carolina at Greensboro

in Partial Fulfillment

of the Requirements for the Degree

Master of Arts

Greensboro

2022

Approved by

Dr. Keith Debbage
Committee Co-Chair

Dr. Wenliang Li
Committee Co-Chair

APPROVAL PAGE

This thesis by Adam Lehman has been approved by the following committee of the Faculty of The Graduate School at The University of North Carolina at Greensboro.

Committee Co-Chair _____
Dr. Keith Debbage

Committee Co-Chair _____
Dr. Wenliang Li

Committee Member _____
Dr. Paul Knapp

____04/01/2022_____
Date of Acceptance by Committee

____03/30/2022_____
Date of Final Oral Examination

ACKNOWLEDGEMENTS

I would like to thank my committee chair, Dr. Keith Debbage for inspiration and guidance on this research project. Additionally, I wish to thank Dr. Wenliang Li and Dr. Paul Knapp for their input and advice regarding remote sensing and climatology. My sincerest thanks to my wife, Stephanie, and daughter, Elizabeth, for their love and support, for which I am eternally grateful, as I worked on this research project.

TABLE OF CONTENTS

LIST OF TABLES……..vi

LIST OF FIGURES……...vii

LIST OF CHARTS…….ix

LIST OF FORMULAS……x

CHAPTER I: INTRODUCTION…….1

Defining Urban Heat Islands……...1
Formation and mitigation of Urban Heat Islands (UHIs)……1
Objectives……4

CHAPTER II: REVIEW OF LITERATURE……...……...……6

A Brief History of UHIs Studies……..……...……...……..6

CHAPTER III: METHODS…..…….…….11

Study sites.…....……..……..……11
Data.....……..……..13
Roof type descriptions……..……..……..……..……...16
Solar radiation, albedo, and emissivity..…….…….……..20
Locations and images of study sites……..……..……..22
Methodology…….....……..……...26
T-test and Pearson product-moment correlation coefficient.....……..…..28
SAS fit plot and regression results…….…...……...…….……....29

CHAPTER IV: RESULTS AND DISCUSSION……..41

CHAPTER V: CONCLUSION……..……...49

REFERENCES……..52

APPENDIX A: RECORDED TEMPERATURE TABLES……..… 60

LIST OF TABLES

Table 1. Spectral Bands of the LandSat 8 TM Sensor……...14

Table 2. Site Names, Designation/Zone, and Roof Type…….…….……....17

Table 3. Radiative properties of natural and manufactured materials……...20

Table 4. Study Site Geographical and Spatial Information..…….....24

Table 5. Dark Albedo Group Roof Type Regression Temperatures…….……...……42

Table 6. Medium Albedo Group Roof Type Regression Temperatures……44

Table 7. Light Albedo Group Roof Type Regression Temperatures……..……...45

Table 8. Averaged temperature ranges by albedo and material……..……..……48

Table 9. Recorded Temperatures in Degrees Fahrenheit °F for the city of Greensboro and study sites with dark albedo...……...…….……60

Table 10. Recorded Temperatures in Degrees Fahrenheit °F for the city of Greensboro and study sites with medium albedo……..61

Table 11. Recorded Temperatures in Degrees Fahrenheit °F for the city of Greensboro and study sites with light albedo……62

LIST OF FIGURES

Figure 1. LandSat 8 Paths and Row for Greensboro, NC……..15

Figure 2. Map of Locations of Study Sites in western Guilford County...……23

Figure 3. Overhead Images of Dark Albedo Sites in western Guilford County...…….24

Figure 4. Overhead Images of Medium Albedo Sites in western Guilford County……..24

Figure 5. Overhead Images of Light Albedo Sites in western Guilford County ……..……25

Figure 6. Fit Plot for USPSDC from December 2019-2020…….....29

Figure 7. Fit Plot for GAB from December 2019-2020……...…….....29

Figure 8. Fit Plot for FEDEX from December 2019-2020…….…….....29

Figure 9. Fit Plot for GIL from December 2019-2020…….....30

Figure 10. Fit Plot for GIL from December 2019-2020.....…….....30

Figure 11. Fit Plot for FASTD from December 2019-2020…….....30

Figure 12. Fit Plot for AP1 from December 2019-2020…….....31

Figure 13. Fit Plot for USPSNDC from December 2019-2020…….....31

Figure 14. Fit Plot for COS from December 2019-2020…….....31

Figure 15. Fit Plot for DE from December 2019-2020…….....32

Figure 16. Fit Plot for HTNS from December 2019-2020……..….....32

Figure 17. Fit Plot for CME from December 2019-2020…….....32

Figure 18. Fit Plot for AP2 from December 2019-2020…….....33

Figure 19. Fit Plot for CAM from December 2019-2020…….....33

Figure 20. Fit Plot for LOW from December 2019-2020…….....33

Figure 21. Fit Plot for HTSS from December 2019-2020…….....34

Figure 22. Fit Plot for HD from December 2019-2020…….....34

Figure 23. Fit Plot for SC from December 2019-2020…….....34

Figure 24. Fit Plot for AH from December 2019-2020…….....35

Figure 25. Fit Plot for WAL from December 2019-2020…….....35

Figure 26. Fit Plot for UNI from December 2019-2020…….....35

Figure 27. Fit Plot for FASTF from December 2019-2020…….....36

Figure 28. Fit Plot for POLO from December 2019-2020…….....36

Figure 29. Fit Plot for BER from December 2019-2020…….....36

Figure 30. Fit Plot for NFI from December 2019-2020…….....37

Figure 31. Fit Plot for AMA from December 2019-2020…….....37

Figure 32. Enlarged image of DE Solar Site with multiple businesses…….44

Figure 33. Before and After Images of HTNS/HTSS and BER study sites to illustrate rooftop changes..……...47

LIST OF CHARTS

Chart 1. Recorded Temperatures in Degrees Fahrenheit °F for the city of Greensboro and Dark Albedo Sites……38

Chart 2. Recorded Temperatures in Degrees Fahrenheit °F for the city of Greensboro and Medium Albedo Sites…..……49

Chart 3. Recorded Temperatures in Degrees Fahrenheit °F for the city of Greensboro and Light Albedo Sites……...……40

LIST OF FORMULAS

Formula 1. Conversion of digital numbers (DN) to radiance……..……..……16

Formula 2. Conversion of radiance to Kelvin (K)……..……..…….16

Formula 3. Conversion of Kelvin (K) to Fahrenheit (F)……..……..……17

Formula 4. Calculating Albedo from LandSat Data Formula……...……..……...22

CHAPTER I: INTRODUCTION

Defining Urban Heat Islands

Urban Heat Islands (UHIs) are a thermal "phenomenon of higher atmospheric and surface temperatures occurring in urban areas compared to the surrounding rural areas" (Xu 2009, 291). These heat islands are a result of sprawling urban landscapes that modify energy absorption, evapotranspiration, and air movements in urban areas (Xu, 2007; Voogi and Oke, 2003).

Understanding the impact of urban warming trends is essential to evaluate their impact and mitigate environmental issues like global warming (Parker, 2010). According to Parker (2010), urban heat islands can differ from city to city as a result of "the different design of the structures and because of the different background climate (p 124). Regardless of scale, the "formation of urban heat islands (UHIs)" creates urban air temperatures that "are higher relative to the natural surroundings" (Debbage and Shepherd 2015, p 181; Oke 1982). The increase in UHIs can be attributed to a combination of growth in urban development (urban sprawl) and the increased frequency of heatwaves due to climatic change (Koomen and Diogo, 2017).

Formation and Mitigation of Urban Heat Islands (UHIs)

UHIs form when there is an observed temperature difference between adjacent urban and rural areas (Memon, Leung, and Liu, 2009). As a global phenomenon, UHIs are most commonly found in highly urbanized locations and can impact local climate and temperatures. Most urban areas are comprised of impervious surfaces (i.e. asphalt, concrete, buildings, structures, etc.) and limited amounts of vegetation. These impervious surfaces contain a high specific heat relative to natural vegetation due to their difference in albedo and emissivity (Memon et al. 2009). Since

2007, there have been several studies that investigate and identify the relationship between UHIs and surrounding landscapes with remote sensing technology (Xu, 2009, p 290).

Location, climate, and meteorological conditions all play important roles in determining the magnitude of UHIs (Theeuwes, Steeneveld, Ronda, and Holtslag, 2017). Synoptic weather patterns and prevailing winds also influence the formation of UHIs (Khaikine, Kuznetsova, Kadygrov, and Miller, 2006). During the summer months (May-August), UHIs in mid-latitude locations like the Piedmont Triad exhibit the greatest fluctuation (Kolokotsa, Psomas, and Karapidakis, 2009). For the Southeastern United States, a synoptic-scale high-pressure cell is the dominant weather feature. These high-pressure cells reduce vertical air movement, while causing light to moderate winds at ground level (Kolokotsa et al. 2009). The reduction in vertical air movement causes additional heat produced by impervious surfaces to become trapped, creating UHIs. Heat stored in impervious surfaces during long summer daytime hours (especially when the air movement is reduced) is generally highest during this period, due to the high angle of the sun and extended daytime hours (Kolokotsa et al. 2009). Research conducted by Kolokotsa et al. (2009) indicated that commercial and industrial land development in the form of urban sprawl, can even impact temperatures at the regional scale.

As research continues to demonstrate the negative impacts of UHIs on local temperatures, urban planners have developed several methods to curb increases in UHIs. While rezoning is not always an option, it is believed that increases in UHIs can be mitigated or prevented through increasing impervious surface albedo (Synnefa, Dandou, Santamouris, and Tombrou, 2008). In recent years, there has been an increased promotion of “cool” roofing technologies as well as a way to help mitigate the UHIs in large urban areas, especially in locations that lack vegetation and surface moisture (Koomen and Diogo, 2017). Some of these

technologies include the creation of more green spaces such as rooftop gardens to provide shade and more evapotranspiration, “cool” roofing and paving coatings to reduce the albedo and enhance the reflectiveness of solar radiation, and the installation of photovoltaic (PV) solar cells for reduction of energy consumption and electrical grid efficiency. When compared to urban parks and green spaces, it is important to remember that the effectiveness of these strategies to mitigate UHIs are limited by their magnitude and spatial distribution (Yang, Xiao, and Ye, 2016).

While the promotion of these strategies and technologies has increased, assessment and analysis of their impact on the UHIs in urban areas have lagged (Barron-Gafford, et al. 2016). To improve urban design and land management, the need to assess the impact of these different strategies is important, as urban planners need to find the correct balance between “urban expansion and thermal environmental quality” which is the essential key to smart growth and sustainable urban planning (Yang, et al. 2020, p 1). As energy consumption is expected to grow by at least 50% by 2050, building more efficient commercial and residential structures represents one of the largest potential solutions to creating a more cost-effective, energy-saving program in metropolitan areas (Casini, 2016, p 3).

Hundreds of cities are currently experiencing the effect of UHIs, and it is expected that this number will continue to increase as developing nations are urban deforestation, urban population increase, and landscape changes with increased urbanization (Qi, He, Wang, Zhu, and Fu, 2019). In some cases, UHIs have been reported with increased temperatures as much as 10 degrees Fahrenheit, which contribute adversely by causing increased energy consumption for air conditioning, decreased air quality, and increased heat mortality (Nichol and Wong, 2005; Santamouris et al. 2016; Lai and Cheng, 2010; Braga, Zanobetti, and Schwartz, 2002;

Mastrangelo et al. 2007; Qi, He, Wang, Zhu, and Fu, 2019). For these reasons, it is easy to see why mitigation of UHIs has become a top priority in many American cities.

Objectives

Analysis and comparison of grey infrastructures (GREIs) in the form of light and dark rooftop infrastructures is an essential aspect of this case study. GREIs are often less commonly accepted options since conventional materials are known to be one of the major causes behind increases in UHIs through their enhanced solar radiation absorptions and the ability for blocking latent heat release (Qi, He, Wang, Zhu, and Fu, 2019). According to Qi, He, Wang, Zhu, and Fu (2019) "Green infrastructures (e.g., green spaces, green walls and roofs, etc.)" have been viewed as important heat sinks necessary to mitigate the effects of UHI, such as natural vegetation (trees) or liquid surface (lakes, ponds, etc.) options are not always available in urbanized areas in arid environments or with limited open space (p 1).

The purpose of this study is to provide a quantifiable measurement of albedo and surface temperature of selected sites in the Greensboro/High Point/Kernersville area, highlighting specific rooftops for analysis and comparison, to provide quantifiable evidence of which roofing technology or technique potentially contributes the least to UHIs of this study area. This study examines the spectral and thermal signatures from different rooftop materials during the late afternoon hour to explore their role in contributing to UHIs. As the urban areas in western Guilford County continue to expand, the impact of increased commercial, industrial, and residential areas will continue to contribute to UHIs in this area.

The promotion of code changes, incentives, and education to promote more "green" buildings has become a major part of urban planning, with cities like Greensboro, High Point,

and Kernersville, becoming a vital part of their Sustainability Action Plans. The use of remote sensing technology will continue to be more important as civil leaders will continue to rely on scientific research to help guide decisions regarding zoning and the development of this area. This study will also prompt more comparative studies as it illustrates the benefits of using remote sensing data in both spatial and temporal analysis, an effort to help mitigate the effects of UHIs in this area.

CHAPTER II: REVIEW OF LITERATURE

A Brief History of UHIs Studies

Since the early 19th century, researchers have been trying to understand the impact of Urban Heat Islands (UHIs). Beginning with large cities, researchers like Luke Howard (1833) in London and Emilien Renou (1862) in Paris have explored the relationship between excess heat in urban areas when compared to the surrounding countryside (as cited in Gartland, 2008, p 1). One of the earliest documented evidence of the urban heat island effect was Charles Caldwell, a physician who lived in Philadelphia in the early 19th century. Caldwell (1798) noted similar temperature differences to that of Howard and Renou, as he documented that Philadelphia often had a summer temperature that was "superior, by three to four degrees, to that of the surrounding country" (48) (as cited in Meyer, 1991, p 39). Although Caldwell was more primarily focused on potential health risks connected with urban life, he noticed that the temperatures between urban and rural areas existed year-round, but were more applicable in the summer month, when cities like Philadelphia became "an artificial torrid zone" compared with cooler temperatures in the countryside (Caldwell, 1801, p 9, as cited in Meyer, 1991, p 39). As Meyer (1991) noted:

> "Brief comments on the nature and causes of the urban climate were common in nineteenth-century journalism, especially during summer heatwaves. For example, the *New York Times* (May 29, 1880, 4) reported: "All other things being equal, great cities are warmer than small cities, on account of the larger heated mass, radiation from the streets, buildings, &c." Those who could afford it began the custom of fleeing to the mountains, the coast, or the countryside in summer to escape" (p 41).

While the earliest American climatologists were aware of the effects of UHIs, they did not find them significant to study other than a unique environmental phenomenon (Meyer, 1991, p 41). The first full-length treatise on American climate came in 1842, by Samuel Forry, who

noted “noted the greater warmth of the urban environment, but saw it principally as a source of error in weather records” (Meyer, 1991, 42). Daniel Draper, while working as the Director of the Central Park Observatory in New York City, first noted a degree of urban warming in 1872, attributing temperature changes to increase urbanization and deforestation (Meyer, 1991, 42).

Serious investigations of the causes, magnitude, and consequences of the urban heat island did not begin to appear in American scientific journals until the early decades of the twentieth century (Meyer, 1991, p 42). The scientific study of urban heat islands in the United States truly began during the mid-20th century, with the work of J. Murray Mitchell as part of the U.S. Weather Bureau in the Office of Climatology (1961). In the *Temperature of Cities* (1961), Mitchell explores the increased heat intensity generated in different urban areas since the 1900s in places like Washington, D.C., Baltimore, MD, and Denver, CO resulting from the outward growth in the urbanized landscape and increased population (p 225).

Since the turn of the century, the size and scale of built-up urban areas in the United States have continually increased, replacing existing vegetation, such that the urban centers are now as warm or warmer than the suburbs (Akbari, Pomerantz, Taha, and Lawrence Berkeley National Lab, 2001). According to Akbari, Pomerantz, Taha, and Lawrence Berkeley National Lab report (2001) “the warming trend became quite obvious, so that, from 1965 to 1989, urban temperatures have increased by about 1°C” (p 295). As a direct result of the increased urban temperatures, there has also been an increase in additional air-conditioning, which is responsible for 5–10% of urban peak electric demand annually costing several billion dollars (Akbari, Pomerantz, Taha, and Lawrence Berkeley National Lab, 2001, p 296). The Lawrence Berkeley National Laboratory studies have “shown that more than 20% of the energy used for air conditioning in the United States could be saved if more reflective surfaces were used in the

urban environment" (Michelsen 1998, p 26). According to Michelsen (1998), this represents a potential energy savings of about 4 billion dollars annually.

In 1963, William Cullen published research conducted for the National Bureau of Standards on built-up roofing (BUR) systems that were exposed to solar heating and radiative cooling. Cullen's findings provided some of the first evidence of the difference in the maximum membrane temperatures between different types of materials, which helped explain the heat capacity of uninsulated and insulated roofing membranes in urban environments (1963, p 4).

Efforts to understand the relationship between albedo and UHIs continued in the 1970s. In 1976, Rossiter and Mathey published a National Bureau of Standards study, "Effects of Insulation on the Surface Temperature of Roof Membranes" which found that the color (more than thickness) of black, gray, and white roofs influenced built-up roofs (BUR) temperatures. While their study focused on the first increment of roofing material, about 1 inch (25 mm), they noted that "increasing the amount of insulation above this first increment to greater thicknesses does not appreciably increase the roof surface temperature" (Rossiter and Mathey, 1976, 15). In a steady-state heat balance, their results did indicate that white roofs exhibited lower surface temperatures than gray or black roofs in some instances by as much as 30 degrees Fahrenheit (Rossiter and Mathey, 1976). One of the limits of this study was its focus on surface temperatures of just black, gray, and white, without a specific albedo range for the roofing materials.

Much of the importance of UHIs was not appreciated until visualization was possible with the development of specially equipped aircraft and advanced satellite technology in the late 1970s (Gartland, 2008, p 7). Explorer Mission 1 (1978) was one of the first satellites equipped with the capacity for thermal heat mapping, enabling the production of remote sensing images

which could demonstrate different surface temperatures (Gartland, 2008, p 7). Thanks to the advances in thermal remote sensing, high-resolution thermal scanners are now able to offer a more discrete way to study diverse urban landscapes (Voogt and Oke, 2003, p 370). Using Advanced Thermal and Land Applications Sensor (ATLAS) to study urbanized and rural areas of Huntsville, AL, Lo, Quattrochi, and Luvall (1997) were able to denote areas of urban heat island impact, noting specific changes either by season or by the time of day.

Using remote sensing technology, various studies have determined the relationship between surface temperatures and weather conditions. While these relationships generally apply only to a specific area, heat islands tend to be strongest during calm, clear summer weather and weakest during cloudy or overcast wintery days (Gartland, 2008, p 7-8). As UHIs are affected by the local scale atmospheric circulation, research studies tend to focus on individual cities (especially those with the fastest rates of urbanization), then regions. By combining Advanced Very High-Resolution Radiometer (AVHRR) satellite data with locally collected temperature and wind intensity data, researchers have learned how calm or moderately windy conditions affect places like Tucson, AZ (Comrie, 2000). As Comrie (2000) noted, "Even with moderate wind speeds, complex temperature patterns are created in the Tucson basin that result from terrain induced flows and heterogeneous land surface characteristics" (p 2430).

Incorporating GIS building shapes with radiometric surface temperatures has enabled researchers to combine two-dimensional images with three-dimensional temperatures ranges (Voogt, 2000, p 21). Combining temperatures with surface components have facilitated a better understanding of the interaction and behavior of various impervious surfaces and UHIs (Voogt 2000). While Voogt's research focused on Vancouver because it possessed a simple urban surface with little vegetation and relatively low buildings, it did demonstrate the capacity of

remote sensing to study urban heat storage and emissivity (30). In 1993, using data from NOAA's 9 and 10 satellites' Advanced Very High-Resolution Radiometer (AVHRR), researcher Hyoun-Young Lee used a regression equation to find a significant correlation between ground surface temperatures and brightness temperatures, using remote sensing to study the intensity of heat islands related the increased population size of cities in South Korea.

Research in the last few decades has been greatly enhanced by the use of remotely sensed thermal infrared (TIR) data, which has become a common source for obtaining land surface temperature (LST) (Corumluoglu and Asri, 2015; Weng et al. 2004; Quattrochi and Luvall, 1999). The widespread distribution of LST data for an entire urban region can now be studied pixel by pixel, with recent developments in high-resolution satellite imaging technologies promising even higher detailed analyses of UHIs (Corumluoglu and Asri, 2015, p 3203). By using a two-dimensional Gaussian surface model superimposed on a planar rural background, Streutker (2002) was able to demonstrate both the magnitude and spatial extent of heat islands near Houston, TX relying solely on satellite data instead of *in situ* information.

Using Moderate Resolution Imaging Spectroradiometer (MODIS) and Advanced Spaceborne Thermal Emission and Reflection Radiometer (ASTER) data, researchers were able to document UHIs through land surface temperatures (LST) in Indianapolis, IN, and its suburbs (Rajasekar and Weng, 2009). Their findings successfully correlated impervious urban surfaces with maximum heat signatures, effectively using both daytime and nighttime satellite images in their analysis (Rajasekar and Weng, 2009). 3-D modeling enabled the identification of two distinct UHIs, which researchers attributed to the rapid development of Marion and Hamilton county attributing increased temperatures to impervious surfaces due to rapid urban development (Rajasekar and Weng, 2009, p 93).

Predicative GIS modeling has allowed researchers to explore regressions between impervious surfaces and populations in an attempt to better understand UHIs patterns. In 2009, Lee and French used high-resolution aerial photography to categorize impervious surfaces as they compared this to employment and population growth in the city of Atlanta, GA. For more than three decades, the Atlanta region has experienced an increase in dispersed suburban developments with the rapid transformation of forest and agricultural land into more urbanized landscapes dominated by impervious surfaces (Lee and French, 2009). The GIS-based estimation method developed by Lee and French (2009) can be used to forecast future amounts of impervious surface developments for other growing metropolitan regions.

Similar research conducted by Debbage and Shepherd (2015) concluded urban contiguity is also a factor that needs to be considered when studying UHIs. Using gridded minimum temperature datasets, Debbage and Shepherd (2015) explored how urban planning could potentially diffuse UHIs through the introduction of more urban greenspaces in several American cities. Their research concluded that contiguous uninterrupted urban footprints both enhance and magnify urban temperatures while illustrating increased urban densities are not a viable UHIs mitigation strategy (Debbage and Shepherd 2015, p 192).

While combining remote sensing technologies and temperature data has been used in several UHIs studies in several locations, none have been applied specifically to large commercial/retail/warehouse buildings in western Guilford County. Conducting a study in this area will be useful because it will offer quantifiable evidence of which roofing system or technology contributes least to UHIs in this area, to mitigate potential temperature increases caused by the current westward urbanized growth pattern in Guilford County.

CHAPTER III: METHODS

Study Sites

The cities of Greensboro, Kernersville, and High Point in Guilford County are ideal urban centers for this study for several reasons. Located in the heart of the Piedmont Triad Region, Greensboro is the third-largest city in North Carolina covering approximately 134.30 sq mi and its location (36.0726° N, 79.7920° W) and size (Population: 296,710) (U.S. Census Estimate, 2019). While High Point and Kernersville areas are smaller (Population: 112,791 covering 57.51 sq mi) and (Population: 24,660 covering 17.89 sq mi) (U.S. Census Estimate 2019) their proximity to Greensboro makes this area an excellent opportunity to study UHIs in a large interconnected urban center in a temperate climate. Over the last three decades, Guilford County has seen a measurable increase in population growth, rising from 421,048 in 2000 to 488,406 in 2010 to an estimated population of 540,521 (U.S. Census Estimate, 2020).

This study area possesses the general characteristics of the Piedmont physiography, with rolling hills and a humid subtropical climate. The typical climatic weather pattern for this area is characterized by hot, humid summers and mild winters. The average high summer temperature is in July, near 90 degrees Fahrenheit with an average low of 68 degrees Fahrenheit. The average winter high and low temperatures occur in January, at 48- and 27-degrees Fahrenheit, respectively. The greatest amount of daylight hours occur in June and July (14.5) with the least amount in December and January (10).

Both spring and fall temperatures create weather conditions that are favorable for the development of thunderstorms, which often occur late in the afternoon. Precipitation is generally well-distributed throughout the year, with a consistent monthly range between 2.9 and 4.8

inches. Guilford County's "landlocked" status also presents an opportunity to study UHIs in an urbanized setting that lies far from any significant body of water.

Data

All three urban areas have several different impervious and non-impervious sites in their urban landscape, which help facilitate easy temperature comparisons. Additionally, most of Guilford County lies completely within two single remote sensing shots taken from the LandSat 8 satellite (Path 16, Row 35 or Path 17, Row 35: See Figure 1), facilitating data collection and analysis. Data collected from LandSat 8 is also ideal because all of the images used are captured at the same time (3:53 pm EDT). Since UHIs are a diurnal cycle (Oke, 1982; Theeuwes, Steeneveld, Ronda, and Holtslag, 2017), the radiometric calibration of these mid-afternoon temperatures represents the greatest amount of solar radiation absorbed by these sites.

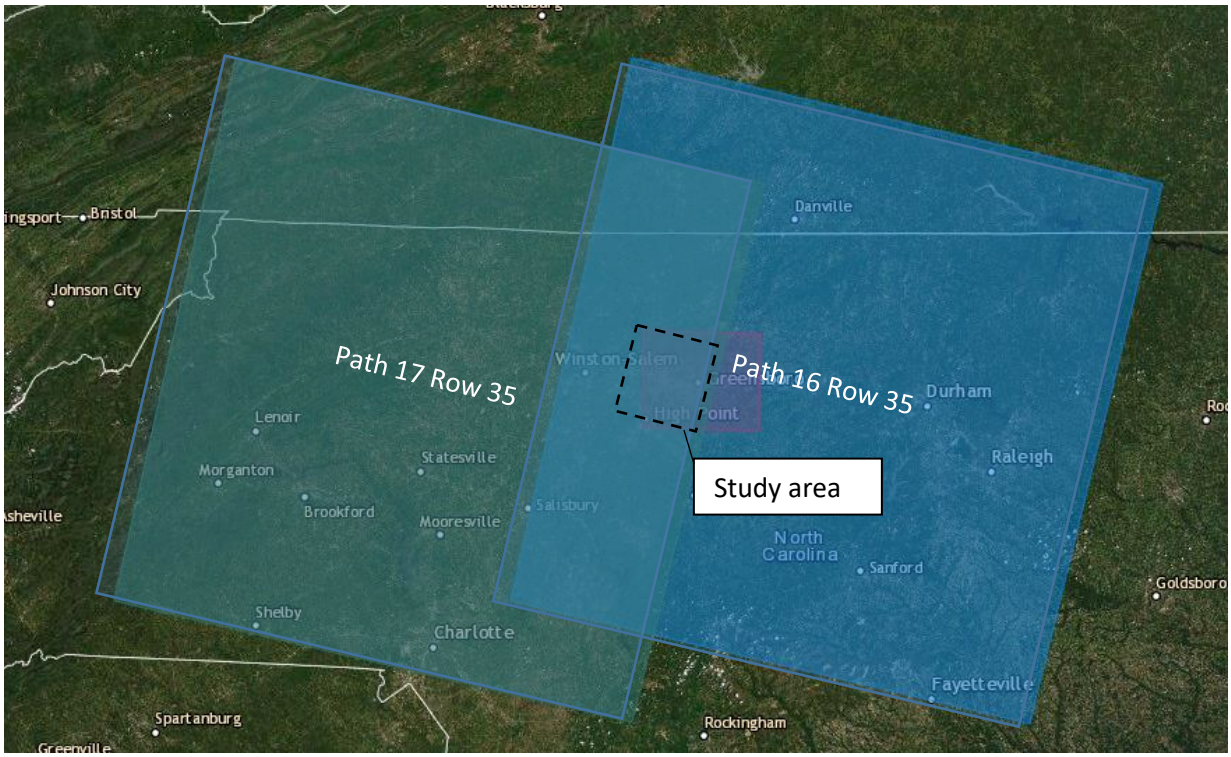

Figure 1: LandSat 8 Paths and Row for Greensboro, NC

Source; United States Geological Survey (USGS) EarthExplorer; 2022

Land surface temperature maps (LSTs) were generated from thermal data obtained from LandSat 8 imagery (band 11 - Thermal Infrared (TIRS) 2 with a wavelength of 11.50-12.51 micrometers and a resolution of 100 meters). LandSat 8 Operational Land Imager (OLI) and Thermal Infrared Sensor (TIRS) images consist of nine spectral bands with a spatial resolution of 30 meters for Bands 1 to 7 and 9. Bands 10 and 11 have a resolution of 100 meters.

Table 1. Spectral Bands of the LandSat 8 TM Sensor

Bands	**Wavelength (micrometers)**	**Resolution (meters)**
Band 1 - Coastal aerosol	0.43-0.45	30
Band 2 - Blue	0.45-0.51	30

Band 3 - Green	0.53-0.59	30
Band 4 - Red	0.64-0.67	30
Band 5 - Near Infrared (NIR)	0.85-0.88	30
Band 6 - SWIR 1	1.57-1.65	30
Band 7 - SWIR 2	2.11-2.29	30
Band 8 - Panchromatic	0.50-0.68	15
Band 9 - Cirrus	1.36-1.38	30
Band 10 - Thermal Infrared (TIRS) 1	10.6-11.19	100
Band 11 - Thermal Infrared (TIRS) 2	11.50-12.51	100

Source; United States Geological Survey (USGS); 2022

Band 11 was used to determine land surface temperatures for these study areas. The thermal remote sensors from this satellite provide spatially averaged temperature values based upon pixel size. LandSat 8 senses radiances measured for each wavelength band and is stored as Digital Numbers (DNs). Since DNs have no unit of measurement, they must be converted to radiance, then converted land surface temperature (LST) in degrees Kelvin. Finally, this Kelvin temperature was converted into degrees Fahrenheit to facilitate temperature comparison between the study sites and the recorded local temperature of Greensboro at the same time and day. The following formulas were derived from the USGS LandSat 8 Handbook (2015) Section 5:

Formula 1. Conversion of digital numbers (DN) to radiance

Float (Band 11)*0.0003342+0.1

Formula 2. Conversion of radiance to Kelvin (K)

1201.14/natural log(480.89)

Using ENVI, these formulas combined into one step:

1201.14/natural log(480.89/(float(Band 11)*0.0003342+0.1)+1)

Formula 3. Conversion of Kelvin (K) to Fahrenheit (F)

$$(K - 273.15) \times 9/5 + 32 = F$$

Roof type descriptions

The all roofing sites in this study share similar construction designs each having a low-sloped roof, which is not completely flat, to prevent "ponding" from snowmelt and rainwater (Ried, 2000, p 15). Large, low-slope roofs are typically found on commercial or industrial buildings (Gartland, 2008, p 46). Approximately one-fourth of all low-slope roofs in the United States are constructed with ethylene propylene diene monomer (EPDM) which is usually a single sheet of synthetic black rubber (Gartland, 2008, p 46). Roofs constructed with EPDM absorb approximately 95 percent of the sun's energy (Gartland, 2008, p 46). Other single-ply materials like polyvinyl chloride (PVC) and thermoplastic polyolefin (TPO) are typically white but the use of these materials represents only about 16 percent of low-sloped roofs. (Gartland, 2008, p 47).

Modified bitumen (approximately 20 percent of low-sloped roofs in the United States) is a membrane composed of asphalt and plastic polymers affixed over an asphalt adhesive layer (Gartland 2008, 46). Typically modified bitumen roofs are dark gray and absorb 80 percent of the sun's energy. Built-up roofing (BUR) represents another 20 percent of low-sloped roofs, comprised of layers of felt or fiberglass mixed with asphalt (Gartland, 2008, p 46). This type of roofing material is usually capped with a layer of small granules or aggregates that are colored tan or gray, absorbing about 75 percent of the sun's energy (Gartland, 2008, p 46). Coated or corrugated metal roofs (CMR) represent a small percentage of low-sloped roofs, despite their

high reflectance and low emissivity (Gartland, 2008, p 46). Based on visual impaction of the site images, the study sites were classified as follows: 1 site EPDM (3.8%), 4 sites as BUR (15.3%), 6 sites as CMR (23.1%), 11 sites as PVC/TPO (42.3%), and 4 sites (15.3%) were classified as composites, using two or more different roofing systems. 15 of the 26 sites (57.7%) are classified as "Industrial/Warehouse" zones and the other 11 sites (42.3%) are classified as "Retail/Commercial" sites, according to the purpose and function of each building.

It is important to remember that high albedo does not guarantee a roofing material will stay cooler (Gartland, 2007, p 60). According to Gartland (2007):

> "Metallic materials such as aluminum coatings can be highly 'reflective' and have a 'high albedo', but they are not cool because of their low thermal emittance. An asphalt shingle can be labeled as 'white' or 'light-colored', but still, have low solar reflectance and gets hot in the sun." (p 60).

Table 2. Site Names, Designation/Zone, and Roof Type

Site Name	**Designation/Zone**	**Roof Type**
Amazon Distribution Center (AMA)	Industrial/Warehouse	PVC/TPO
Atlantic Packaging (AP1)	Industrial/Warehouse	CMR
Atlantic Packaging (AP2)	Industrial/Warehouse	BUR/PVC/TPO
DE Solar (DE)	Industrial/Warehouse	PVC/TPO
Gilbarco Veeder-Root (GIL)	Industrial/Warehouse	CMR
Fastenal Distribution Center (FASTD)	Industrial/Warehouse	BUR
Fastenal Fulfillment Center (FASTF)	Industrial/Warehouse	PVC/TPO
Federal Express (FEDEX)	Industrial/Warehouse	CMR

GTCC Center for Advanced Manufacturing (CAM) (formally the Thomasville Bus Factory)	Industrial	PVC/TPO
Harris Teeter Distribution Center (North Side) (HTNS)	Industrial/Warehouse	CMR
Harris Teeter Distribution Center (South Side) (HTSS)	Industrial/Warehouse	PVC/TPO
NFI Hanes Brand (NFI)	Industrial/Warehouse	PVC/TPO
Polo Ralph Lauren Services Center	Industrial/Warehouse	BUR/ PVC/TPO
US Postal Service Network Distribution Center (USPS-NDC)	Industrial/Warehouse	BUR
US Postal Service Distribution Center (USPS-DC)	Industrial/Warehouse	EPDM
At Home (AH)	Retail/Commercial	PVC/TPO
Bernard's Furniture Group (BER)	Retail/Commercial	BUR/ PVC/TPO
Costco (COS)	Retail/Commercial	CMR
CME Crown Mark (CME)	Retail/Commercial	CMR
Gabes (GAB)	Retail/Commercial	BUR
GBF Medical Group (GBF)	Retail/Commercial	BUR
Home Depot (HD)	Retail/Commercial	PVC/TPO
Lowe's Home Improvement (LOW)	Retail/Commercial	CMR/PVC/TPO
Sam's Club (SAM)	Retail/Commercial	PVC/TPO
Walmart (WAL)	Retail/Commercial	PVC/TPO
Universal Furniture (UNI)	Retail/Commercial	PVC/TPO

Additionally, each of these buildings in this study is unaffected by shadowing effects from any nearby taller structures and is classified as either retail/commercial or industrial/warehouse by the Greensboro Zoning Department. All but four of these buildings are

free-standing structures as both the Harris Teeter Distribution Center (North Side) and (South Side) and Fastenal Fulfillment Center and Polo Ralph Lauren Services Center are connected. Each of these sites was selected because of its size (greater than 100,000 square feet/10,000 square meters). The average surface area for these buildings is approximately 292,705 square feet (27,193 square meters). 11 of these buildings (42.3%) are above the average, with the Amazon Distribution Center (AMA) being the largest, covering approximately 1 million square feet.

The average age of these buildings is close to 26 years, with a majority (18) (69%) being older than the average age. Lifespans for large buildings in this study (industrial, commercial, warehouses) vary from 20 to 40 years, with the low slope roofs typically guaranteed to last between 5 and 25 years before being replaced (Reid 2000, 21). The oldest building in this study is the GTCC Center for Advanced Manufacturing (CAM) which was constructed in 1969 and repurposed from the Thomasville Bus Company in 2019.

Table 3. Radiative properties of natural and manufactured materials

Surfaces	**Albedo Ranges**	**Emissivity Ranges**
Natural		
Forest	.13-.20	.90-.99
Grass	.16-.26	.90-.98
Sand	.20-.45	.84-.92
Snow	.50-.90	.82-.99
Manufactured		
Asphalt	.05-.27	.89-.96
Brick	.20-.60	.90-.92
Concrete	.10-.35	.85-.97
Corrugated metal	.10-.16	.13-.28
White paint	.50-.90	.85-.95

Source: Stewart, I. D., and Mills, G. M. (2021). *The Urban Heat Island: a guidebook*. Elsevier, (p 17); Oke, T. R., Mills, G., Christen, A., Voogt, J.A., (2017) *Urban Climates*. Cambridge University Press.

Solar Radiation, Albedo, and Emissivity

Solar radiation can be transmitted (passing through), absorbed (resulting in heating), or scattered (redirected) (Stewart and Mills, 2021, p 17). Interaction with a medium defines what happens to the energy transmitted, as a medium's ability to absorb solar radiation is equal to its ability to emit the same wavelength (Stewart and Mills, 2021, p 17). According to Stewart and Mills (2021), "For an opaque solid there can be no transmission and all scattering occurs away from its surface as a reflection 17). Emissivity is defined as a ratio of energy that radiates from a medium compared to a perfect emitter (i.e. blackbody), under the same temperature and wavelength, ranging between 0 and 1.0.

Albedo is an important property of the Earth's surface representing the average reflectance of the sun's spectrum (Liang, 2000; Smith, 2010). Albedo, like emissivity, is a

unitless quantity, with values that range from 0 to 1.0. This value varies based on the land cover, as a snowpack would have a high value whereas an evergreen forest would have a low value (Liang, 2000; Smith, 2010). Using the following LandSat formula below (developed by Liang (2000) and normalized by Smith (2010)), shortwave albedo can be calculated:

Formula 4. Calculating Albedo LandSat Formula

$$\alpha_{short} = \frac{0.356\rho_1 + 0.130\rho_3 + 0.373\rho_4 + 0.085\rho_5 + 0.072\rho_7 - 0.0018}{0.356 + 0.130 + 0.373 + 0.085 + 0.072}$$

The following band math formula in ENVI was used to calculate the albedo ranges for this study:

((0.356*B1 (Coastal Aerosol)) + (0.130*B2 (Blue)) + (0.373*B3 (Green)) + (0.085*B4 (Red)) + (0.072*B5 (Near Infrared)) -0.018) / 1.016. Sites were categorized through a supervised classification method, based on the lowest range of their albedo (dark: albedo < .25; medium: albedo between .26 and .47 and light: albedo >.48). The range in albedo for the study sites was from .07 to .65.

The categorical classifications in this study are relative and subjective, as terms like "dark", "medium", and "light" do not have a definitive mathematical scale. Efforts to use this type of classification stem directly from Rossiter and Mathey's (1976) study, as they classified the rooftops as "black", "gray", or "white" without a specific corresponding albedo range for the roofing materials. Using discrete groupings facilitates comparison between different albedos and roofing materials preventing the muddling of charts and graphics with too much information.

Locations and Images of Study Sites

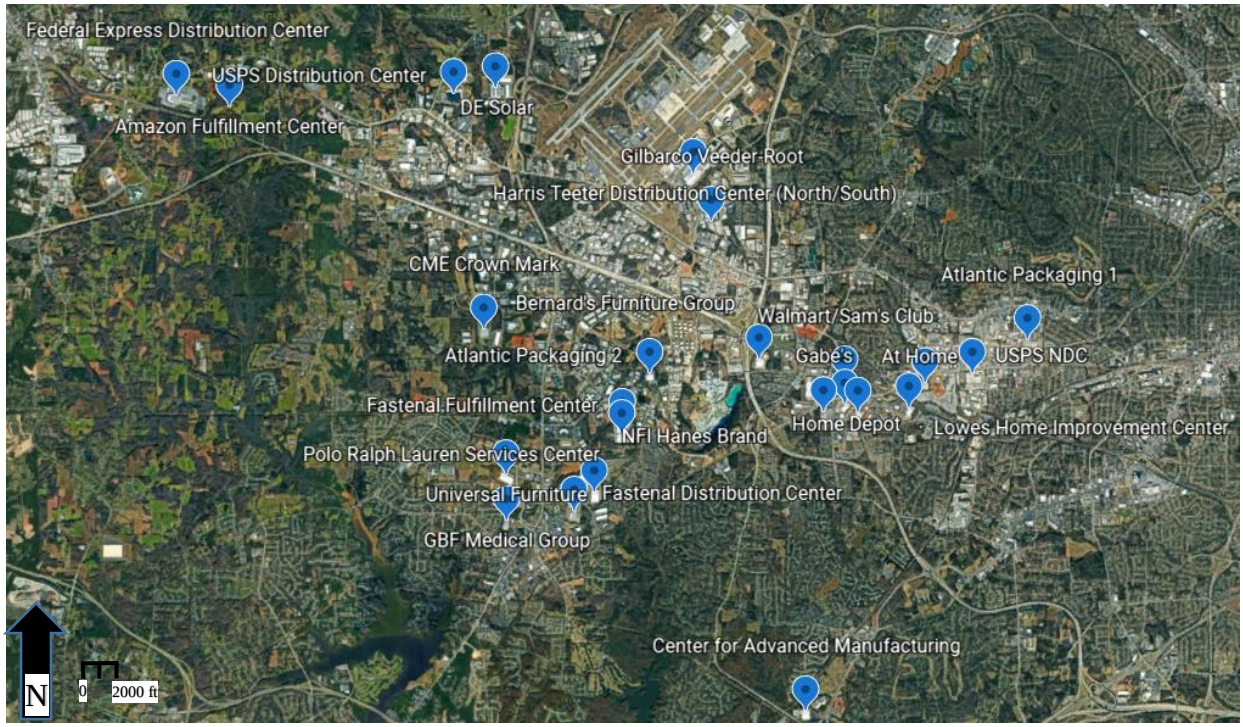

Figure 2. Map of Locations of Study Sites in western Guilford County

Source; Google Earth; 2022

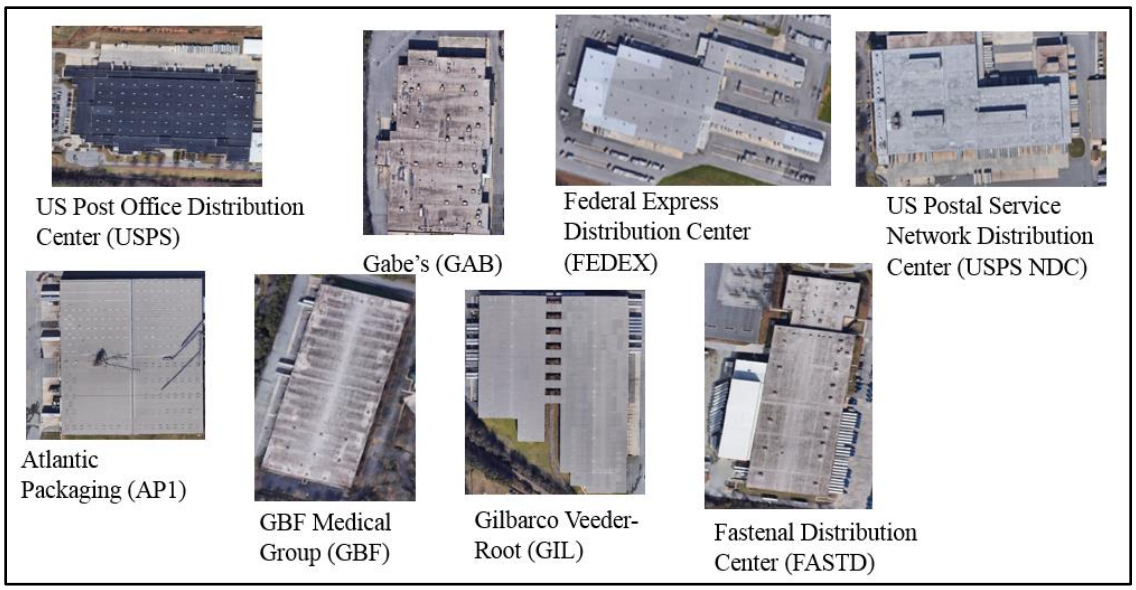

Figure 3. Overhead Images of Dark Albedo Sites in western Guilford County

Source; Google Earth; 2022

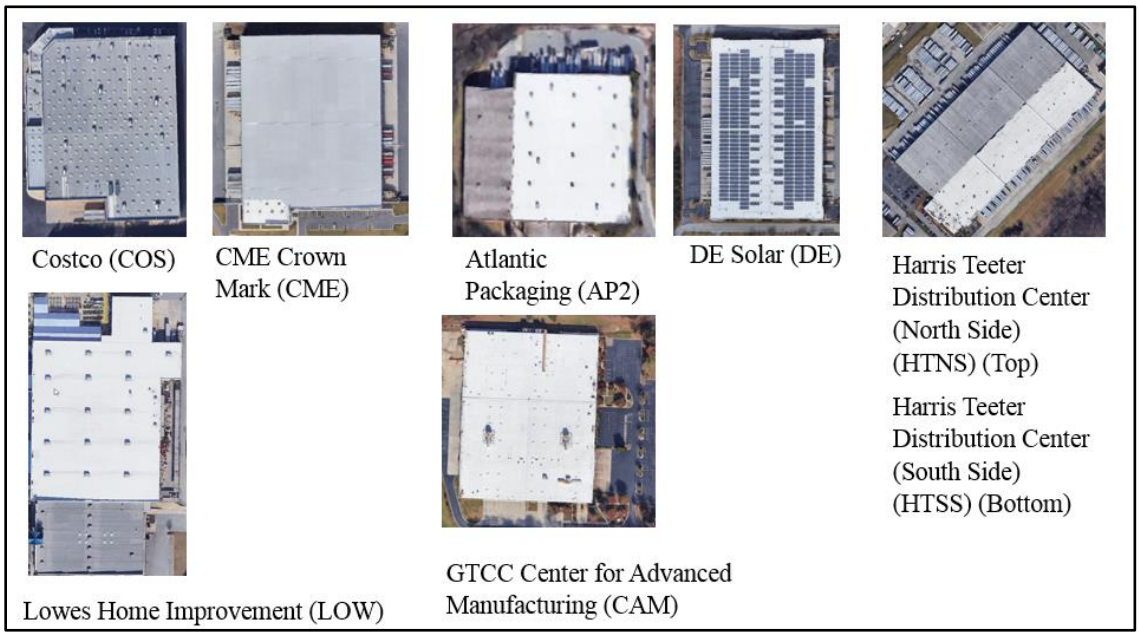

Figure 4. Overhead Images of Medium Albedo Sites in western Guilford County

Source; Google Earth; 2022

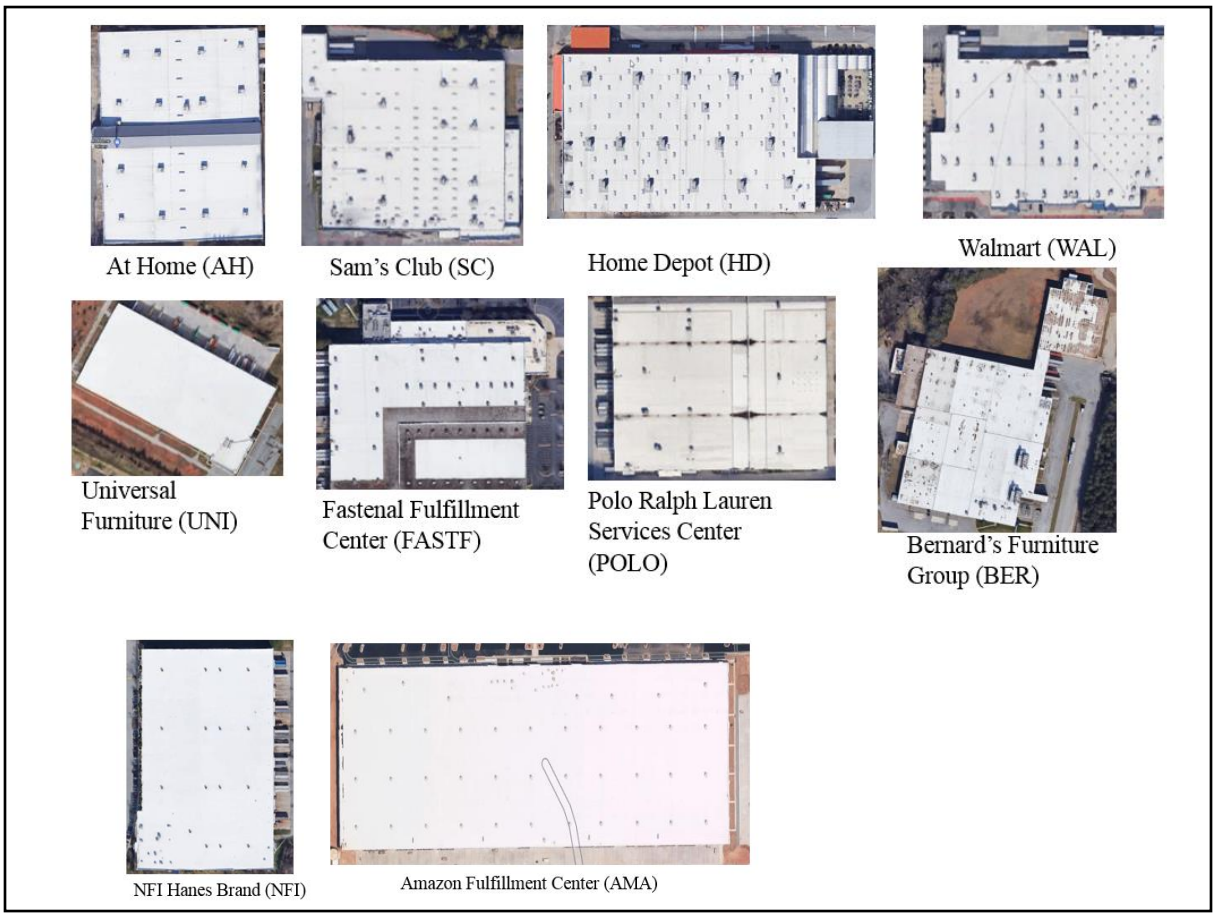

Figure 5. Overhead Images of Light Albedo Sites in western Guilford County

Source; Google Earth; 2022

Table 4. Study Site Geographical and Spatial Information

Albedo Range	**Category**	**Site Name**	**Year Built**	**Latitude/ Longitude**	**Approximate Area**	
					(in sq ft)	**(in sq m)**
.07-.08	Dark	USPS Distribution Center (USPS-DC)	2000	36° 6' 23" N 79° 59' 08" W	452,354	42,025
.15-.19	Dark	Gabe's (GAB)	1994	36° 3' 10" N 79° 54' 14" W	178,349	16,569
.16-.18	Dark	Federal Express (FEDEX)	2010	36° 5' 25" N 80° 2' 09" W	483,000	44,872
.17-.19	Dark	Gilbarco Veeder-Root (GIL)	1986	36° 5' 04" N 79° 55' 32" W	355,137	32,993
.21-.28	Dark	Atlantic Packaging (AP1)	1979	36° 3' 50" N 79° 51' 45" W	153,935	14,302
.21-.23	Dark	GBF Medical Group (GBF)	1990	36° 2' 09" N 79° 58' 10" W	228,969	21,272
.22-.24	Dark	Fastenal Distribution Center (FASTD)	1994	36° 2' 14" N 79° 57' 20" W	297,353	27,625
.24-.28	Dark	USPS-Network Distribution Center (USPS-NDC)	1972	36° 3' 31" N 79° 52' 26" W	295,247	27,429
.26-.27	Medium	Costco (COS)	2003	36° 3' 26" N 79° 53' 01" W	147,071	13,663
.26-.44	Medium	DE Solar (DE)	2006	36° 6' 19" N 79° 58' 13" W	422,466	39,248
.26-.44	Medium	Lowe's Home Improvement (LOW)	1993	36° 3' 11" N 79° 53' 11" W	139,702	12,979
.28-.31	Medium	Harris Teeter Distribution Center (North Side) (HTNS)	1973	36° 5' 34" N 79° 55' 49" W	304,504	28,289
.32-.34	Medium	CME Crown Mark (CME)	2018	36° 4' 03" N 79° 58' 24" W	268,737	24,966
.35-.58	Medium	Atlantic Packaging (AP2)	1989	36° 3' 34" N 79° 56' 23" W	194,270	18,048
.45-.46	Medium	Center for Advanced Manufacturing (CAM)	1969	35° 59' 57" N 79° 55' 14" W	280,112	26,023

.48-.51	Light	Harris Teeter Distribution Center (South Side) (HTSS)	1973	36° 5' 33" N 79° 55' 49" W	251,606	23,375
.48-.52	Light	Home Depot (HD)	1993	36° 3' 35" N 79° 53' 58" W	142,718	13,259
.48-.51	Light	Sam's Club (SAMS)	1992	36° 3' 28" N 79° 54' 02" W	139,524	12,962
.49-.54	Light	At Home (AH)	1994	36° 3' 09" N 79° 53' 50" W	125,331	11,644
.51-.52	Light	Wal-Mart (WAL)	1992	36° 3' 26" N 79° 53' 55" W	203,081	18,867
.58-.60	Light	Universal Furniture (UNI)	2006	36° 2' 36" N 79° 58' 10" W	333,760	31,007
.52-.54	Light	Fastenal Fulfillment Center (FASTF)	1990	36° 3' 05" N 79° 56' 45" W	235,343	21,864
.52-.54	Light	Polo Ralph Lauren Services Center (POLO)	1990	36° 2' 59" N 79° 56' 45" W	326,240	30,309
.56-.59	Light	Bernard's Furniture Group (BER)	1970	36° 3' 40" N 79° 55' 00" W	294,397	27,350
.58-.60	Light	Universal Furniture (UNI)	2006	36° 2' 36" N 79° 58' 10" W	333,760	31,007
.60-.62	Light	NFI Hanes Brand (NFI)	2002	36° 2' 25" N 79° 57' 06" W	357,112	33,176
.61-.65	Light	Amazon Distribution Center (AMA)	2018	36° 6' 18" N 80° 1' 27" W	1,000,000	92,903

Methodology

The process of determining whether a region of interest exists in a given image can be divided into two steps: feature extraction and classification (Siddula, Dai, Ye, and Fan, 2016, p 372). Features from an image can be extracted into spectral (e.g. RGB color, contrast, filter, and wavelength), spatial (e.g. size, shape, and texture), and topological features (continuous deformations) (Siddula, Dai, Ye, and Fan, 2016, p 372; Tsai, 2007; Riedmiller et al. 2012; Zhang et al. 2006; Belongie et al. 2002; Prasad et al. 2006; Rothwell, et al. 1996; He, et al. 2009; Kim, 2012). Using data retrieved from USGS LandSat 8, a post-classification comparison evaluated relative surface temperatures for each site for each month, ranging from December 25, 2019 to December 27, 2020 to capture monthly/seasonal temperature variations.

This post-classification comparison allows for the spectral classification of each of the spatial images for each site on different dates, but at the same time of day. Using a post-classification similar to Streuker's (2003) study, each satellite image was be selected based upon availability and cloud cover (less than 25%) to provide the most accurate comparison for solar radiation absorption. Of the 46 images available from USGS LandSat 8 for the period, only 23 met that criteria for this study.

Each image has been being separately classified by date and time to minimize errors in radiometric calibration. Using ENVI software, surface temperature has been calculated and converted from Kelvin into Fahrenheit, then subtracted from the record high temperature for Greensboro for the same date and time. By comparing the data from each of these areas, this study can offer some insight into which roofing technology or technique potentially contributes the least to the area's UHIs. The control temperature (local Greensboro temperature) is the

reported temperature from the weather station at the Piedmont Triad International Airport (published online by WeatherUnderground [www.wunderground.com]).

T-Test and Pearson product-moment correlation coefficient

This case study uses a two-tailed independent sample t-test to determine the statistical distribution of each of the temperature sets, as well as illustrate any kurtosis in the data. All of these data sets have leptokurtic distributions, with each having a wider or flatter shape with fatter tails. All of these data sets have a Pr > |t| value of .001, which is below the necessary threshold α-value of 0.05 for significance. If the α-value is below the threshold of 0.05, then the null hypothesis (H_O) (i.e. solar radiation does not influence rooftop temperatures) can be rejected in favor of the alternative hypothesis (H_A):

$$H_O: \mu_{tL} = \mu_{tH}$$

$$H_A: \mu_{tL} = \mu_{tH}$$

The second part of this research used the Pearson product-moment correlation coefficient (Pearson's correlation) to measure the correlations between the recorded high temperature for the city of Greensboro (taken at the PTI airport) (independent variable) and the radiometric calibrated temperature derived from the LandSat 8 image with ENVI (dependent variable). Utilizing a non-parametric correlation test generated by a SAS program, there is a positive linear correlation between the recorded high temperature for Greensboro and radiometrically calibrated temperatures for each study site at the same time and date. With a p-value of <.001 (which is below .05 alpha level) the null hypothesis is rejected, as the result is statistically significant. The fit plot diagrams (see below) illustrate the regression:

SAS Fit Plot and Regression Results

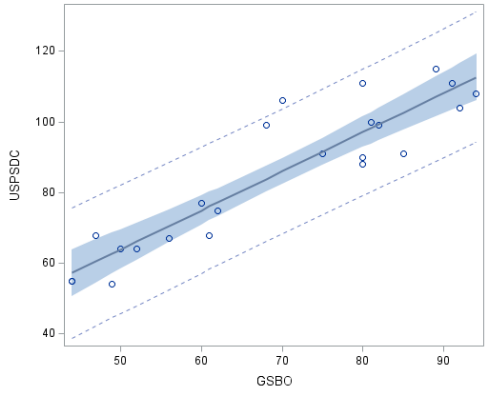

Observations	23
Parameters	2
Error DF	21
MSE	69.33
R-Square	0.8385
Adj R-Square	0.8308

Figure 6. Fit Plot for USPSDC from December 2019-2020

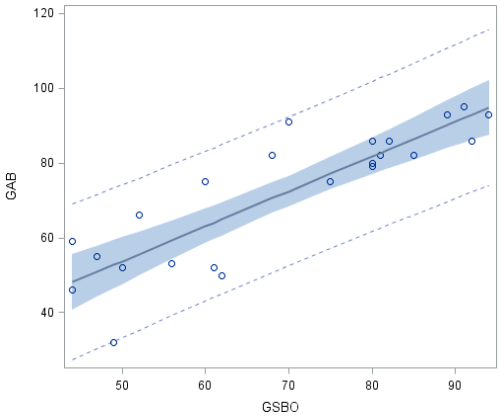

Observations	23
Parameters	2
Error DF	21
MSE	87.47
R-Square	0.745
Adj R-Square	0.7329

Figure 7. Fit Plot for GAB from December 2019-2020

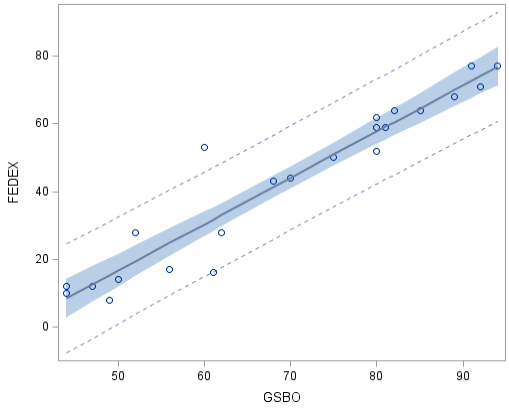

Observations	23
Parameters	2
Error DF	21
MSE	52.317
R-Square	0.9131
Adj R-Square	0.9089

Figure 8. Fit Plot for FEDEX from December 2019-2020

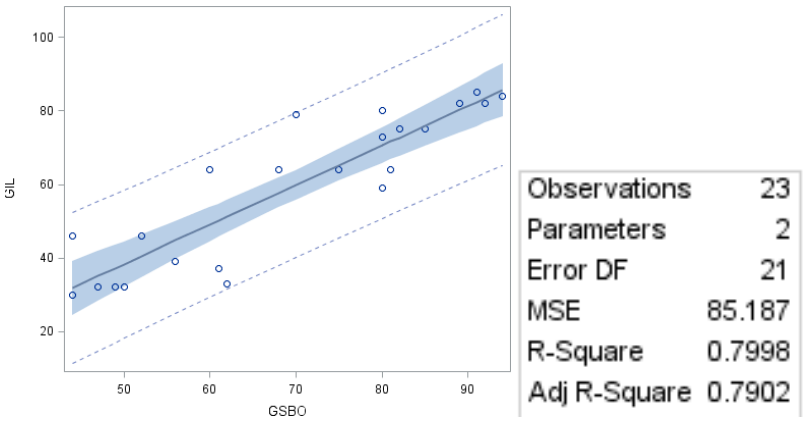

Figure 9. Fit Plot for GIL from December 2019-2020

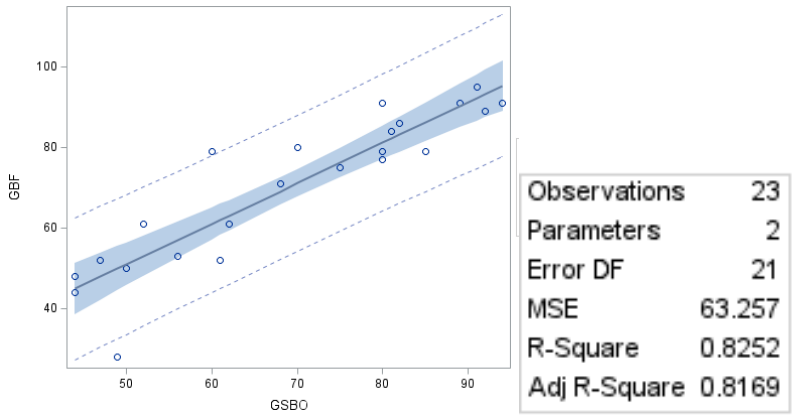

Figure 10. Fit Plot for GIL from December 2019-2020

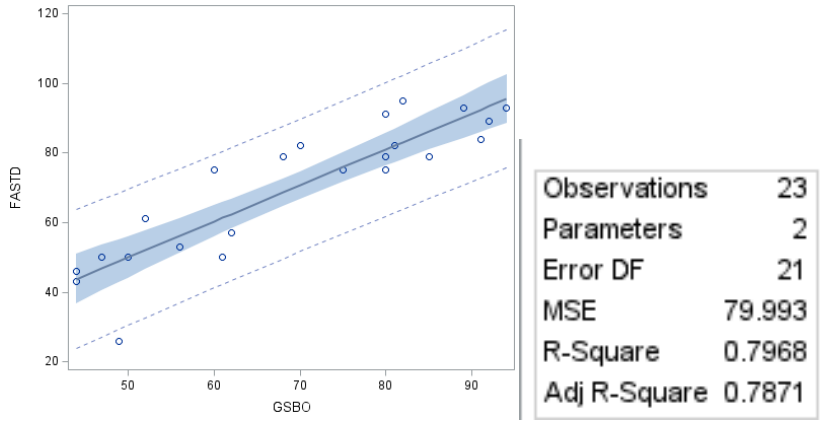

Figure 11. Fit Plot for FASTD from December 2019-2020

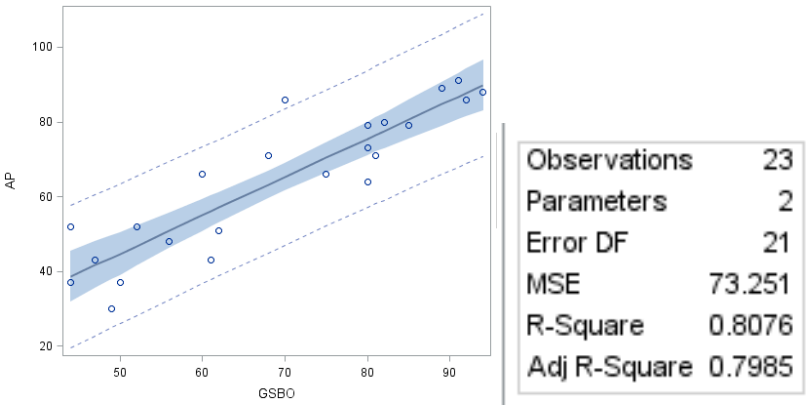

Figure 12. Fit Plot for AP1 from December 2019-2020

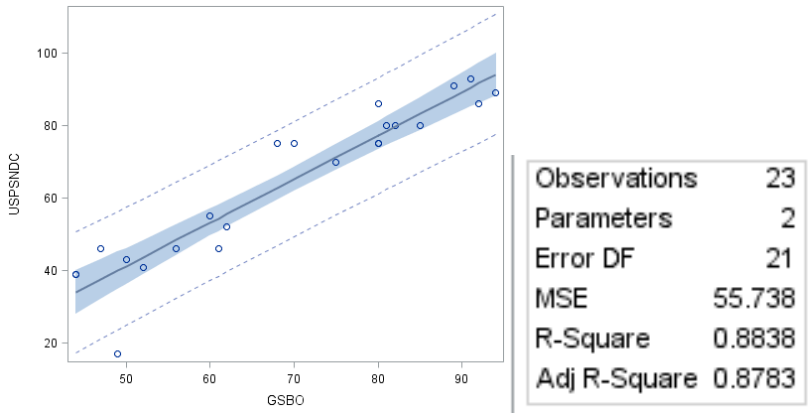

Figure 13. Fit Plot for USPSNDC from December 2019-2020

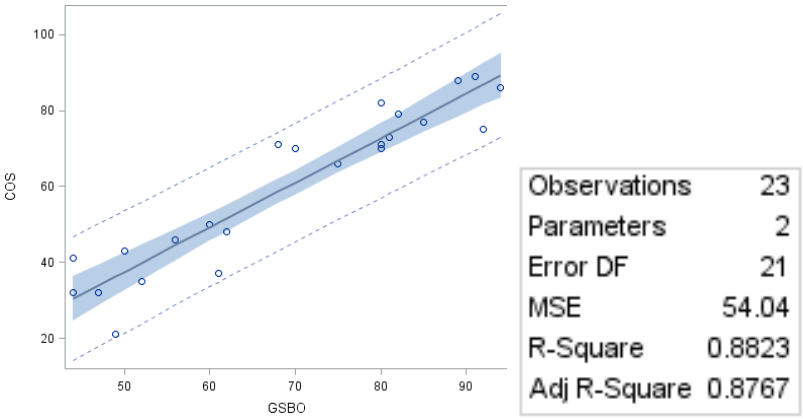

Figure 14. Fit Plot for COS from December 2019-2020

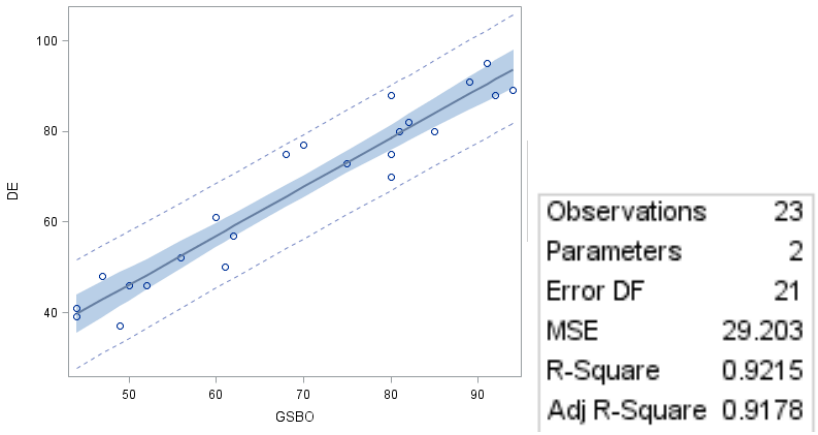

Figure 15. Fit Plot for DE from December 2019-2020

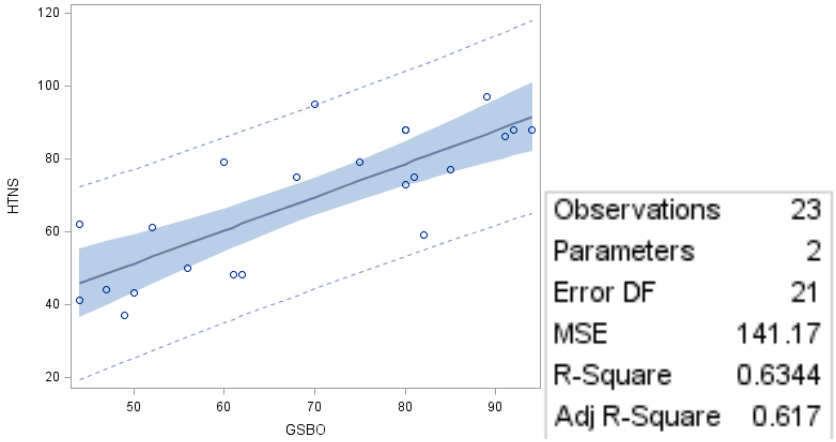

Figure 16. Fit Plot for HTNS from December 2019-2020

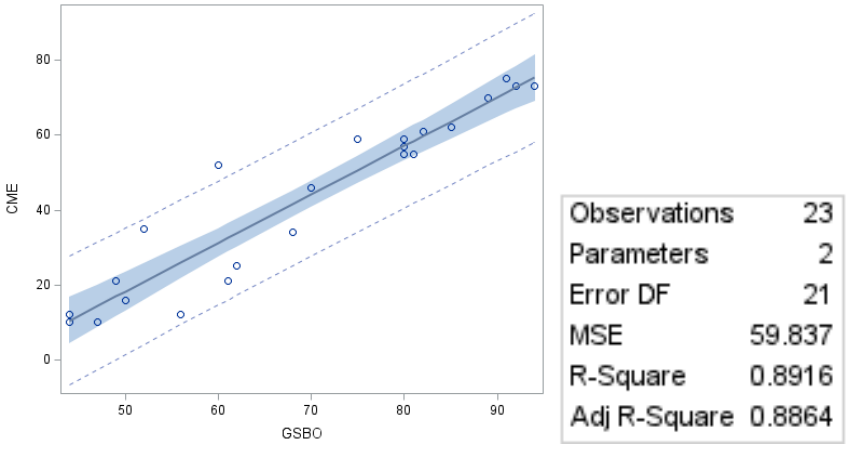

Figure 17. Fit Plot for CME from December 2019-2020

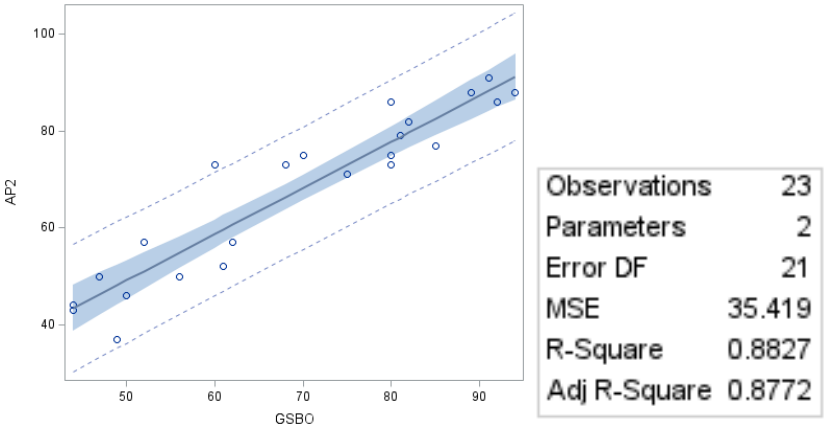

Figure 18. Fit Plot for AP2 from December 2019-2020

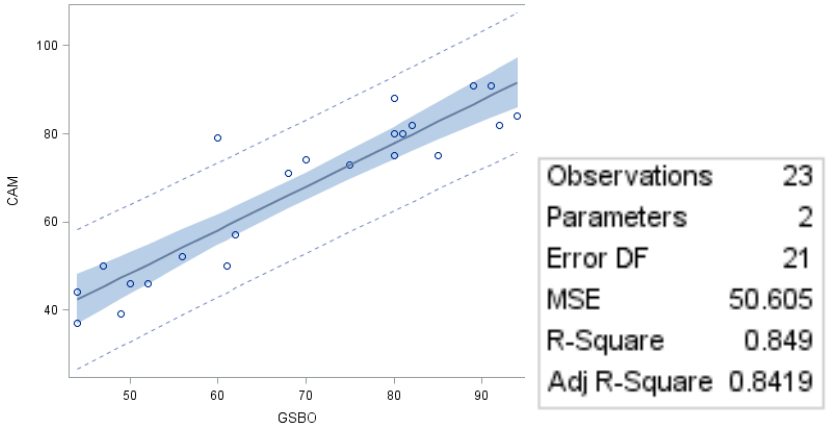

Figure 19. Fit Plot for CAM from December 2019-2020

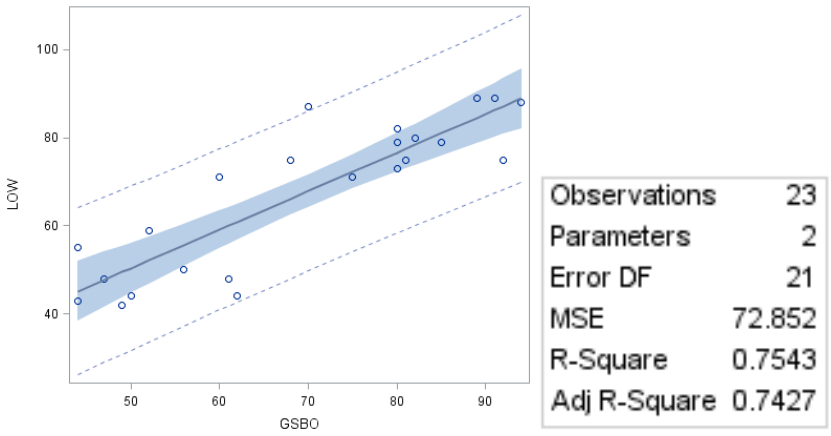

Figure 20. Fit Plot for LOW from December 2019-2020

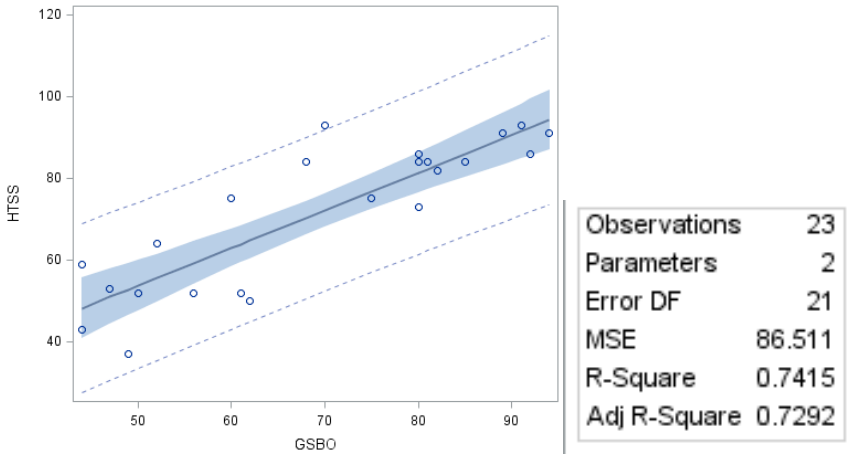

Figure 21. Fit Plot for HTSS from December 2019-2020

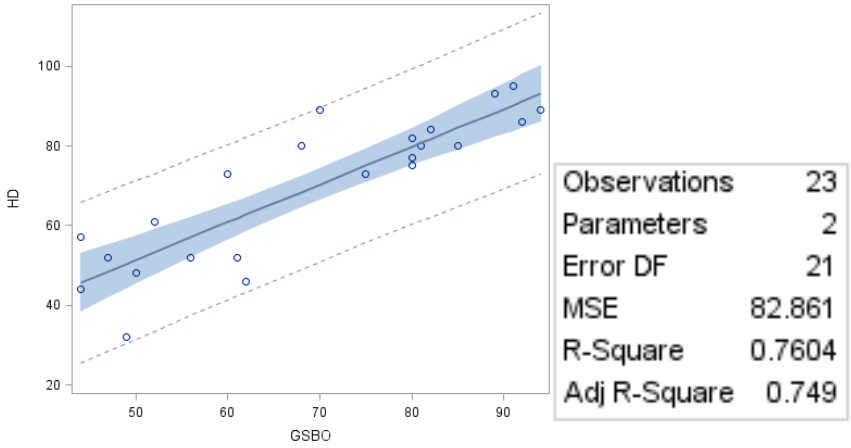

Figure 22. Fit Plot for HD from December 2019-2020

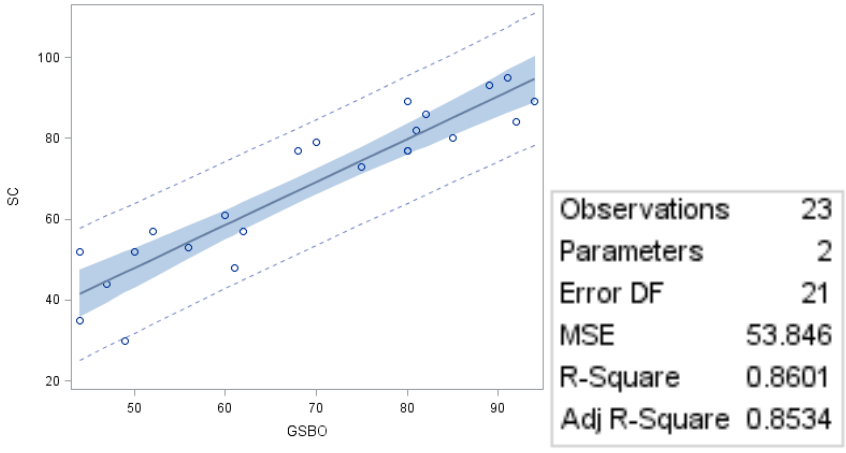

Figure 23. Fit Plot for SC from December 2019-2020

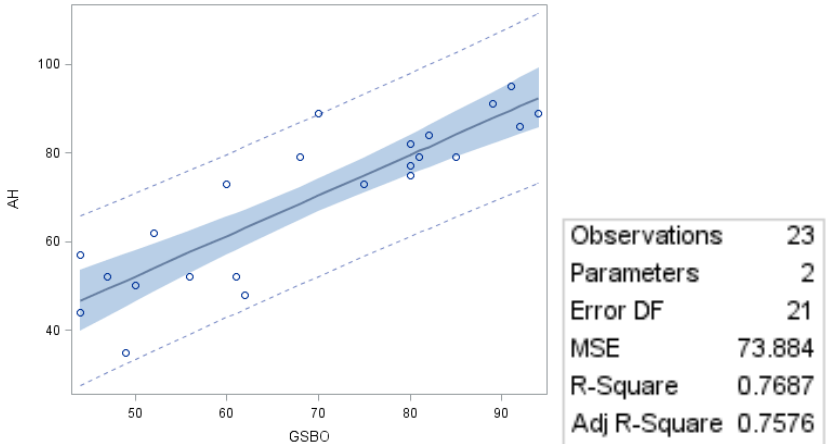

Figure 24. Fit Plot for AH from December 2019-2020

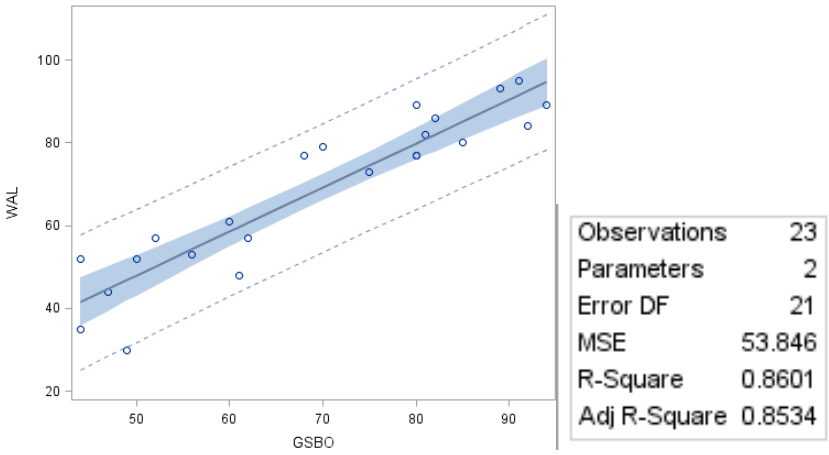

Figure 25. Fit Plot for WAL from December 2019-2020

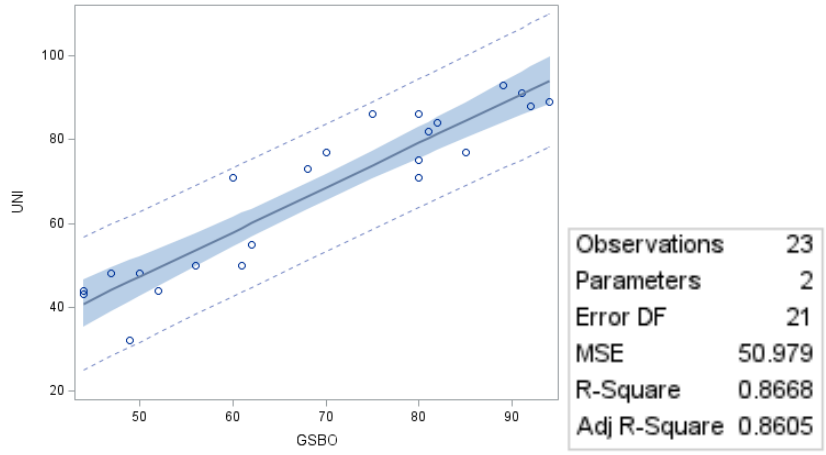

Figure 26. Fit Plot for UNI from December 2019-2020

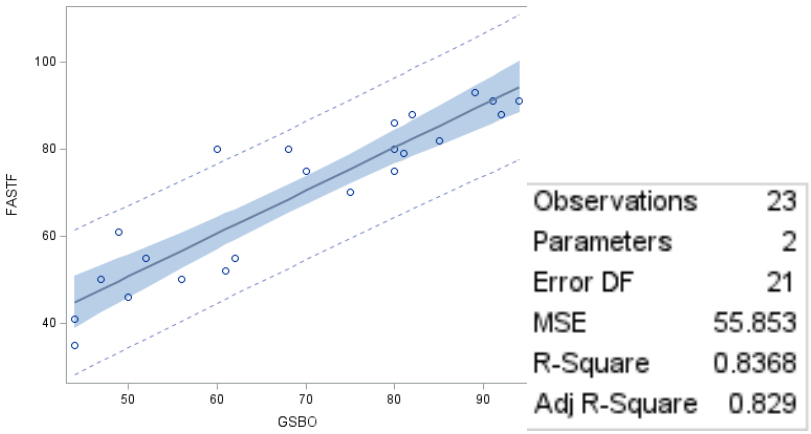

Figure 27. Fit Plot for FASTF from December 2019-2020

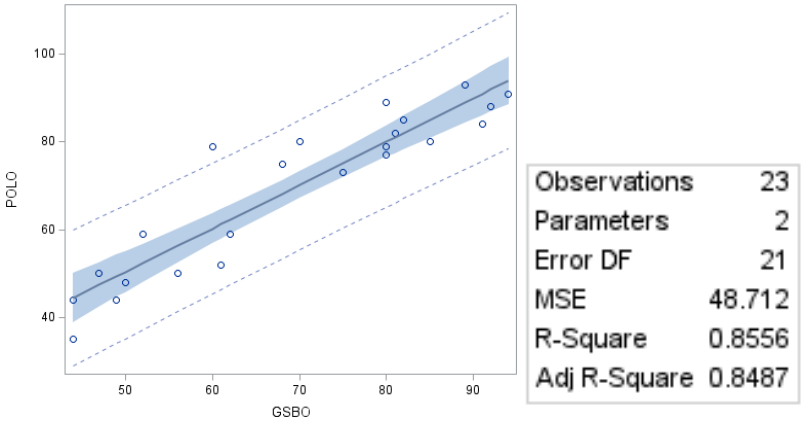

Figure 28. Fit Plot for POLO from December 2019-2020

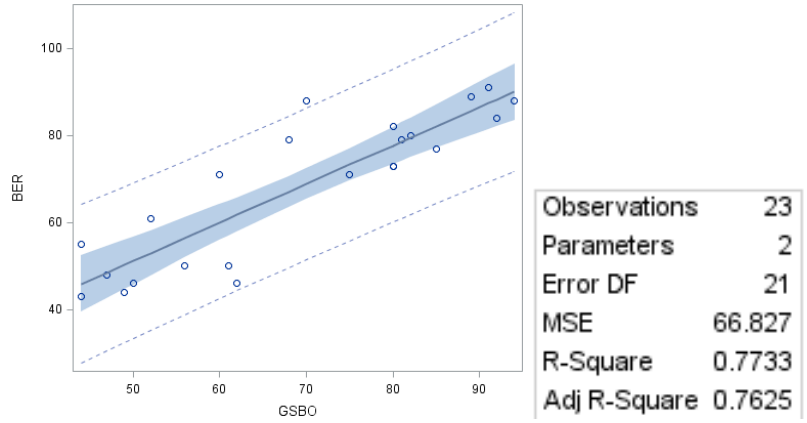

Figure 29. Fit Plot for BER from December 2019-2020

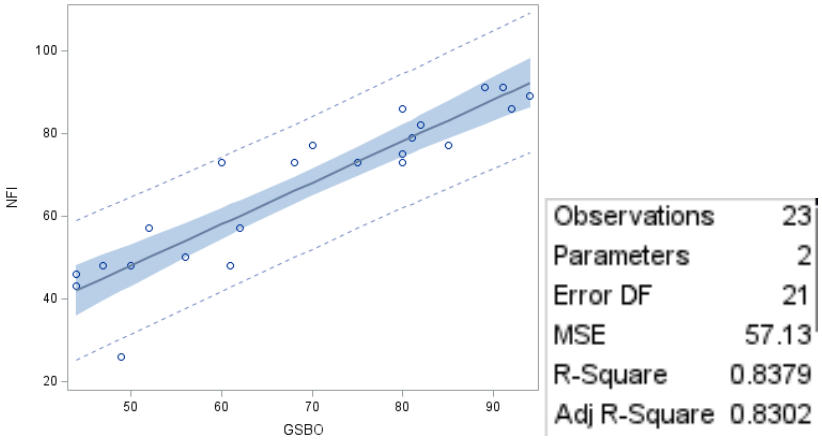

Figure 30. Fit Plot for NFI from December 2019-2020

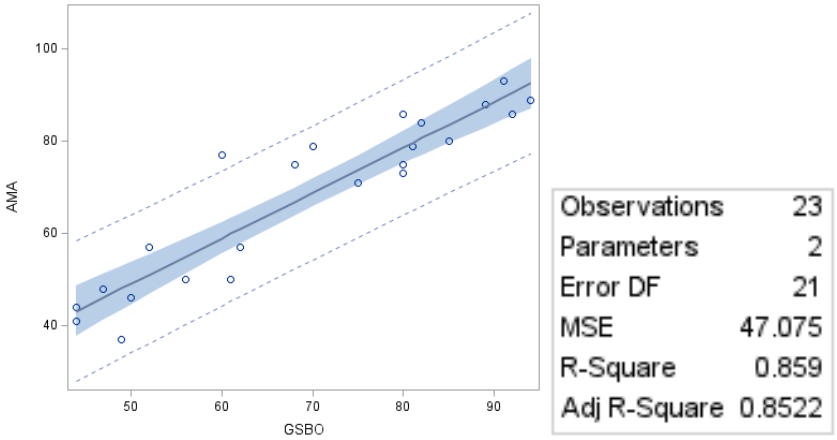

Figure 31. Fit Plot for AMA from December 2019-2020

Chart 1. Recorded Temperatures in Degrees Fahrenheit °F for the city of Greensboro and Dark Albedo Sites

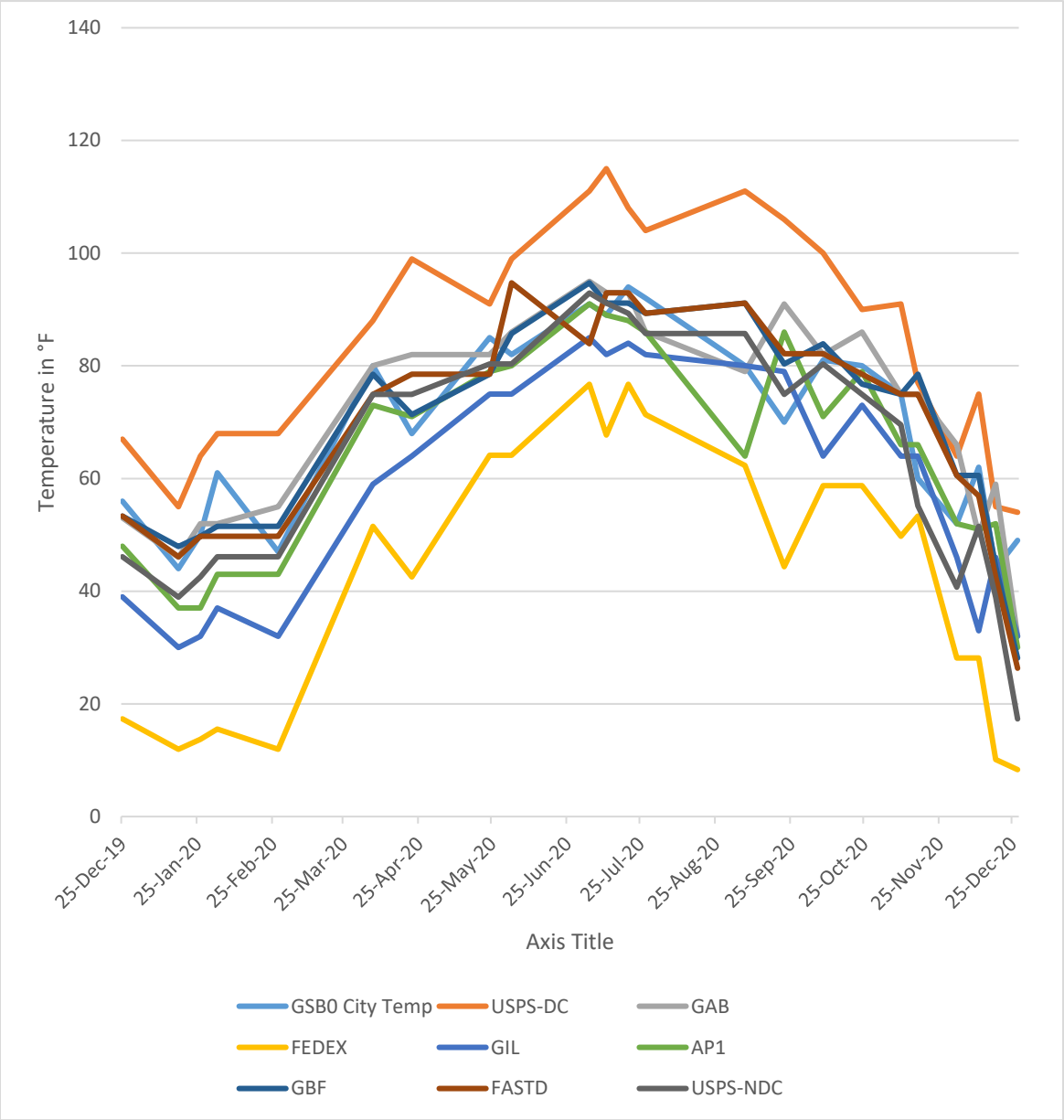

Chart 2: Recorded Temperatures in Degrees Fahrenheit °F for the city of Greensboro and Medium Albedo Sites

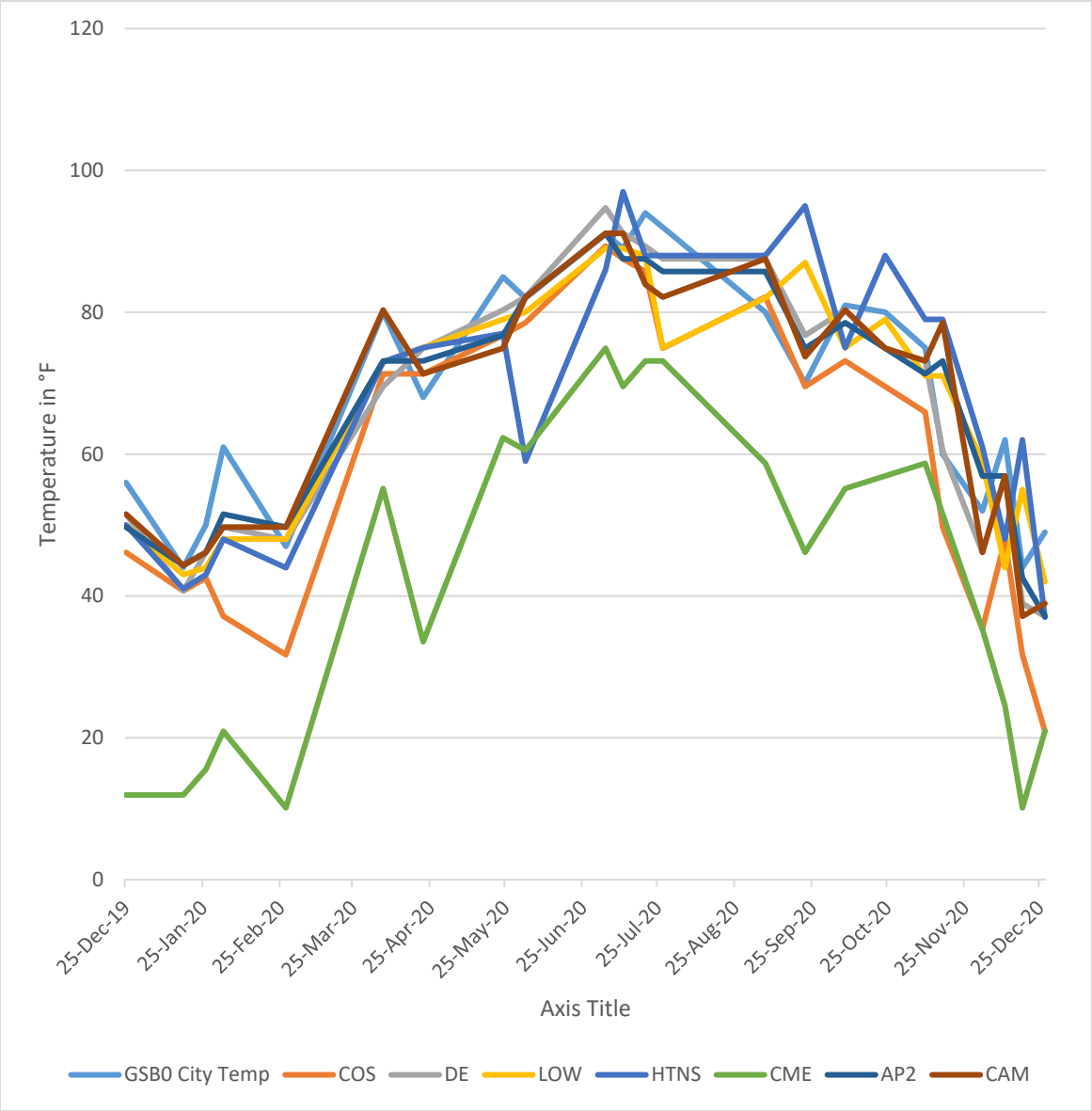

Chart 3: Recorded Temperatures in Degrees Fahrenheit °F for the city of Greensboro and Light Albedo Sites

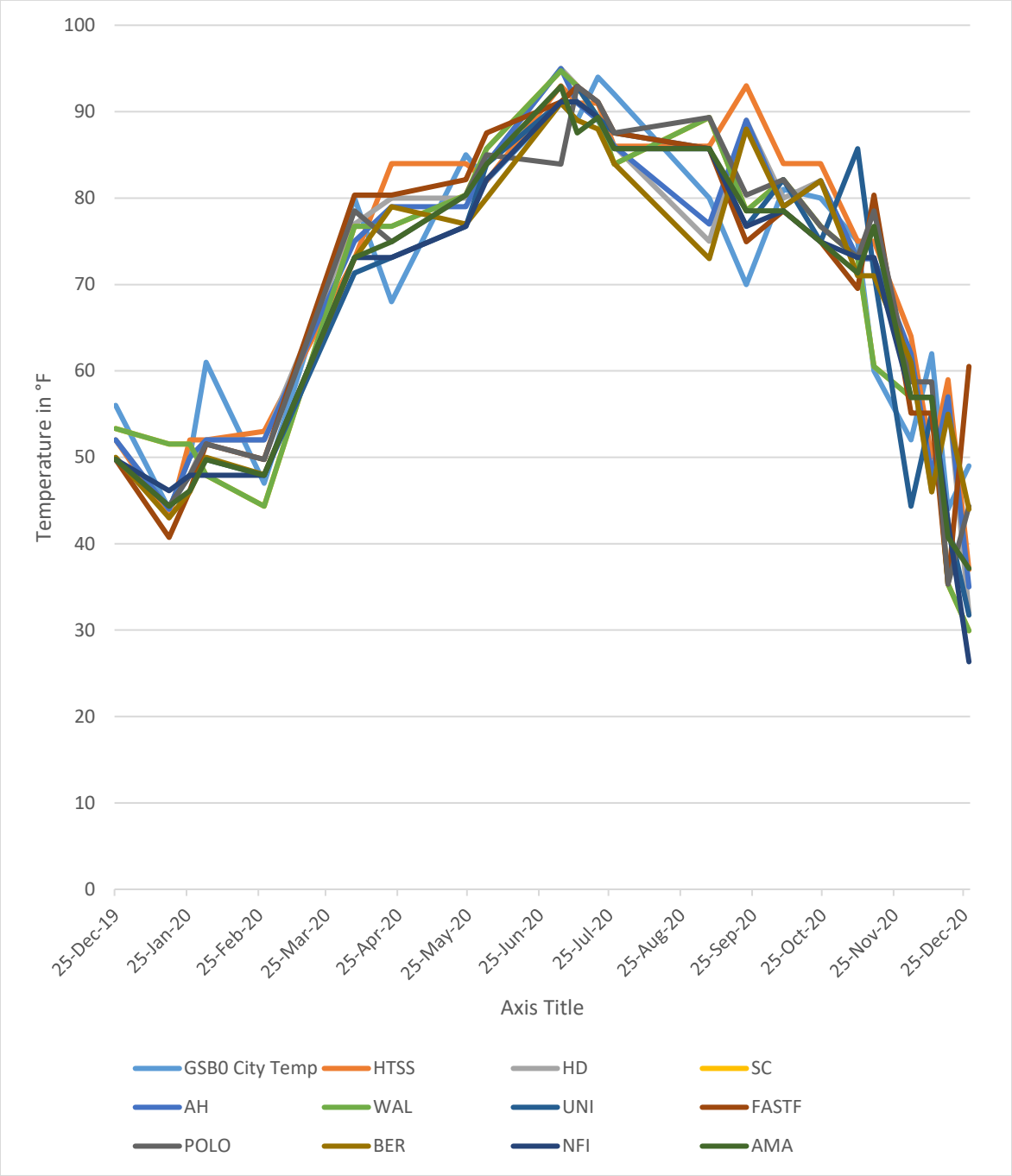

CHAPTER IV: RESULTS AND DISCUSSION

This study provided quantifiable measurements of albedo and surface temperature of selected sites in western Guilford County, which enabled the analysis of specific rooftops for comparison. By examining the spectral and thermal signatures from different rooftop materials during the late afternoon, this study found several interesting trends related to both albedo and roofing materials.

Starting with the dark albedo group, these had the sites with both the lowest and highest surface temperatures (FEDEX and USPSDC), as well as having the greatest range in variation between temperatures between sites and the Greensboro temperature (-51.87 to 8.5 degrees Fahrenheit). Across four different seasons, the outlier sites (FEDEX and USPSDC) remain consistently either above or below the Greensboro city temperature respectively (see Chart 1 and Table 5 below). Since these two buildings have similar square footage and functions (i.e. warehouse), it seems more likely that their differences in roofing material account for the temperature variation. Additionally, the shape of the FEDEX building may also contribute to its lower temperatures, as the entire surface area of the rooftop is irregular and not a uniform polygon.

Three out of four of the lowest surface temperatures in the dark albedo group had similar roofing materials, either coated or corrugated metal roofing (CMR) as opposed to built-up roofing (BUR) or ethylene propylene diene monomer (EPDM) roofs. These findings seem to match with the research of Qi et al. (2019), who noted: “color and material types have significant influences on material albedo change, while surface texture and thickness have limited impacts.

Therefore, color and construction material should be emphasized in practical UHIs mitigation" (6).

While all roofing sites in this study did share similar construction shapes of low-sloped roofs, there is possible evidence of "ponding" rainwater (potential rusting or discoloration of sections of the CMR roofing) which could contribute to their lower temperatures (Ried, 2000). The CMR materials in this study could be affected by this, as more solar energy is required to evaporate moisture before the rooftop temperature increases.

Table 5: Dark Albedo Group Roof Type Regression Temperatures

Site	Roof Type	Regression Line (Degrees Fahrenheit)
FEDEX	CMR	-51.87 + (1.4 * GSBO Temp) (95% confidence level)
USPSNDC	BUR	-19.0 + (1.2 * GSBO Temp) (95% confidence level)
GIL	CMR	-15.6 + (1.1 * GSBO Temp) (95% confidence level)
AP1	CMR	-6.5 + (1.0 * GSBO Temp) (95% confidence level)
FASTD	BUR	-1.74 + (1.0 * GSBO Temp) (95% confidence level)
GBF	BUR	+.38 + (1.0 * GSBO Temp) (95% confidence level)
GAB	BUR	+7.1 + (1.0 * GSBO Temp) (95% confidence level)
USPSDC	EPDM	+8.5 + (1.1 * GSBO Temp) (95% confidence level)

In the medium albedo group, the range is less severe (-46.52 to 6.7 degrees Fahrenheit) than that of the dark albedo group. Once again, roofing materials appear to explain the differences in the surface temperature ranges. The coated or corrugated metal roofing materials performed better than either the polyvinyl chloride (PVC) or thermoplastic polyolefin (TPO), with two outliers (See Table 6 below).

One of the anomalies of this group is the Harris Teeter North Side (HTNS) building. HTNS is one of the sites that is not a free-standing building (it is physically connected along its longitudinal axis to the Harris Teeter South Side (HTSS)) and its temperature readings are influenced by the resolution of the aggregated pixel size used in this study. The Lowes Home

Improvement store (LOW) is comprised of three different building materials, which inhibits a discrete surface temperature reading also due to the resolution of aggregated pixel size from the LandSat 8 satellite. One of the more confounding effects in this study is related to the varied or composited roofing construction for several of the study sites as this affected the overall rooftop albedo and temperature of these study sites.

One of the most surprising results from this study was the DE Solar site, which is a multi-purpose warehouse facility, home to several businesses: Lewis Logistics (shipping), Carson-Dellosa Publishing Group (education supply wholesaler), Momentum Textiles (upholstery shop), and Dedon Inc. (outdoor furniture store) in addition to being a 1.3-megawatt solar power plant (U.S. Energy Information Administration, 2022). Approximately 57% of this rooftop, 244,000 square feet (22,668 square meters) of 422,466 square feet (39,248 square meters) available is covered with 244 photovoltaic solar panels (each representing about 1,000 square feet each with an albedo of .24) (See Figure 32 below). Although this dark albedo was a severe contrast with DE Solar's PVC/TPO rooftop albedo of .44, this seems to provide a marginal effect on the overall rooftop temperature, as DE Solar's recorded temperatures were consistent with similar albedos and roofing materials in the light albedo group.

These findings correspond with the results reported by Salamanca et al. (2016), as they investigated the surface temperature effects of photovoltaic solar panels and discovered that their temperatures were only a few degrees warmer than "cool" (lighter albedo) roofs in the Phoenix and Tucson metropolitan areas. While cool roofs "were more effective at cooling than rooftop solar panels…solar panels are more efficient at reducing the nocturnal UHI magnitude…therefore more directly [able to] combat effects associated with urban development" (Salamanca et al. 2016, p 218).

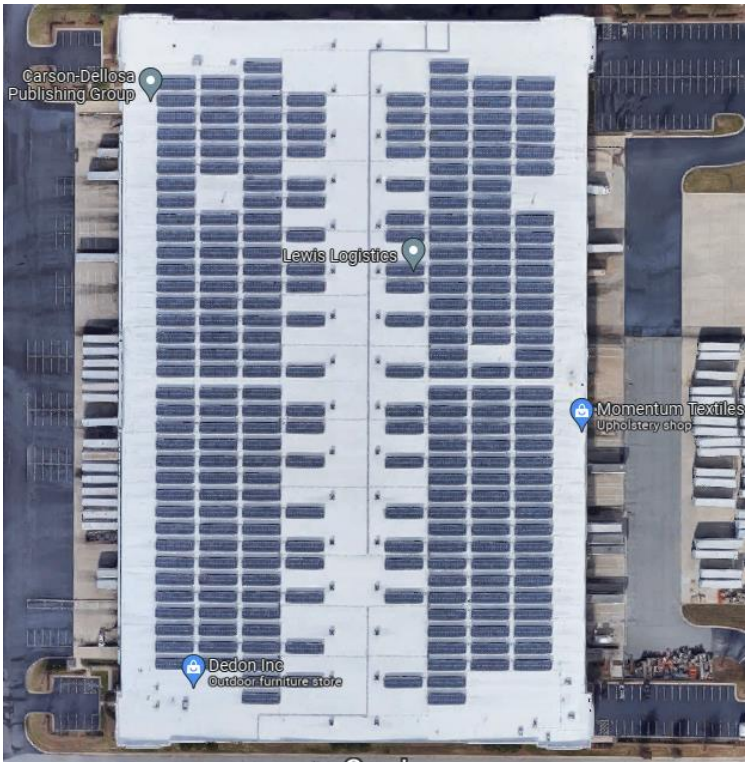

Figure 32. Enlarged image of DE Solar Site with multiple businesses
Source; Google Earth, 2022

Table 6: Medium Albedo Group Roof Type Regression Temperatures

Site	Roof Type	Regression Line (Degrees Fahrenheit)
CME	CMR	-46.52 + (1.3 * GSBO Temp) (95% confidence level)
COS	CMR	-21.3 + (1.2 * GSBO Temp) (95% confidence level)
DE	PVC/TPO	-7.9 + (1.0 * GSBO Temp) (95% confidence level)
CAM	PVC/TPO	-1 + (1.0 * GSBO Temp) (95% confidence level)
AP2	BUR/PVC/TPO	+1.49 + (0.95 * GSBO Temp) (95% confidence level)
HTNS	CMV	+5.5 + (1.0 * GSBO Temp) (95% confidence level)
LOW	CMR/PVC/TPO	+6.7 + (0.9 * GSBO Temp) (95% confidence level)

The light albedo group has the least variation between its study sites (-5.95 to +7.7 degrees Fahrenheit) (See Table 7). A distinct temperature difference for all light albedo sites can be noted for February 2, 2020, as the Greensboro temperature was much higher than the temperatures recorded for this group on this day. A possible explanation for the rooftop

temperature difference could stem from the previous overnight temperatures from February 1, 2020 (overnight low temperature of 36 degrees Fahrenheit and moderate winds on February 2 with gusts up to 24 mph accompanied by light rainfall of .20 inches).

Two other outliers occurred on April 22 and September 22, when the light albedo site temperatures were higher than the Greensboro recorded temperature. Temperatures for the preceding days (April 21 and September 21) were about 5 degrees Fahrenheit warmer, with a higher overnight temperature. This could have compromised this group's ability to cool off completely before the next day. This matches the expectations reported by Gartland (2008), as UHIs tend to be weakest during overcast or wintery days. Additionally, these anomalies seem to be influenced by moderate wind speeds, similar to those reported by Comrie (2000) in his study of Tucson, AZ.

Table 7: Light Albedo Group Roof Type Regression Temperatures

Site	Roof Type	Regression Line (Degrees Fahrenheit)
UNI	PVC/TPO	-5.95 + (1.1 * GSBO Temp) (95% confidence level)
SC	PVC/TPO	-5.3 + (1.1 * GSBO Temp) (95% confidence level)
WAL	PVC/TPO	-5.3 + (1.1 * GSBO Temp) (95% confidence level)
NFI	PVC/TPO	-2.19 + (1.0 * GSBO Temp) (95% confidence level)
AMA	PVC/TPO	-.42 + (0.99 * GSBO Temp) (95% confidence level)
POLO	BUR/ PVC/TPO	+.70 + (0.99 * GSBO Temp) (95% confidence level)
FASTF	PVC/TPO	+1.28 + (0.99 * GSBO Temp) (95% confidence level)
HD	PVC/TPO	+4.0 + (0.95 * GSBO Temp) (95% confidence level)
AH	PVC/TPO	+6.3 + (0.92 * GSBO Temp) (95% confidence level)
BER	BUR/ PVC/TPO	+7.1 + (0.90 * GSBO Temp) (95% confidence level)
HTSS	EDPM/PVC/TPO	+7.7 + (0.90 * GSBO Temp) (95% confidence level)

The rooftop coating can also explain some of the temperature variations between roofing materials. Given the similar roofing material construction and albedo, this group had two odd potential outliers, Bernard's Furniture Group (BER) and Harris Teeter South Side (HTSS). As a feature of building renewal, rooftop maintenance is a key feature for large buildings. Coating

large rooftops with lightweight PVC or TPO materials have negligible influences on loads of existing structures while reducing the relative albedo.

Despite being in the lightest albedo group and having very high albedos, both the Harris Teeter Distribution Center (South Side) (HTSS) and Bernard's Furniture Group (BER) had some of the highest surface temperatures for the light albedo group, which illustrates some advantages of roof coating and as well as its limitations. As Gartland (2008, p 60) stated, having a high albedo does not guarantee a lower surface temperature. This can be seen in Figure 33, as the dark albedo EPDM roofing on both buildings has been covered over with a light albedo PVC or TPO material. If the covered EPDM materials are similar to those used by the United States Parcel Service Distribution Center (USPSDC), then the lighter albedo may account for the slightly cooler surface temperature. Such coating methods are one of the most popular and widespread techniques used in the United States (Akbari et al. 2006 as cited in Qi et al. 2019, p 8).

HTNS/HTSS (Before (Left) and After (Right) 2019)

BER (Before (Left) and After (Right) 2019)

Figure 33. Before and After Images of HTNS/HTSS and BER study sites to illustrate rooftop changes

Source; Google Earth and Guilford County GIS Office; 2022

In both the dark and medium albedo groups of this study, coated/corrugated metal roofing performed well throughout the year, representing some of the lowest surface temperatures when compared to the official recorded temperature of the city of Greensboro and other roofing

materials. In this regard, the material composition appears to influence roof temperature more than albedo, even though these materials were darker in color. Although darker colors generally absorb more energy than light colors, the emissivity of the roofing material played a significant role in the lower remote sensed surface temperature.

Additionally, there are several confounding effects related to composite rooftop construction (rooftops comprised of two or more different materials). This affected the overall rooftop temperature and albedo for four of these study sites. Functionality (retail/commercial vs industrial/warehouse) could also be a factor, as this could influence the internal temperatures and insulation of these buildings.

Overall, while lighter colored materials tend to absorb less solar radiation, the roofing material prevented them from having the lowest surface temperatures. While the light albedo group did not have the lowest surface temperatures, this group did have the least variation between the minimum and maximum temperatures, as compared to either the dark or medium albedo groups over one year (see Table 8 below).

Table 8. Averaged temperature ranges by albedo and material

Averaged Temperature Ranges by Albedo:	
Dark albedo group (8 sites):	-9.84 + (1.1 * GSBO Temp)
Medium albedo group (7 sites):	-9.0 + (1.0 * GSBO Temp)
Light albedo group (11 sites):	+.80 + (.99 * GSBO Temp)
Averaged Temperature Ranges by Material	
EPDM (1 site):	+8.5 + (1.1 *GSBO Temp)
BUR (4 sites):	-3.315 + (1.05 * GSBO Temp)
CMR (6 sites):	-22.72 + (1.16 * GSBO Temp)
PVC/TPO (11 sites)	+1.13 + (1.0 * GSBO Temp)
Composite (More than two materials) (4 sites)	+3.99 + (.94 * GSBO Temp)

CHAPTER V: CONCLUSION

Based on the findings of this study, many of the rooftop materials performed as expected. In all cases, there was a positive correlation between Greensboro temperature and all of the roofs in this case study. As earlier research by Qi, et. al. (2019) predicted, innovative GREIs do appear to increase solar reflectivity and latent heat release (2). As temperatures in the late summer and early fall were the highest, the findings in this study also connect with conclusions drawn from previous researchers (i.e. Oke, 1982; Voogt, 2000; Oke and Voogt 2008; Gartland, 2008) regarding the greatest potential for UHIs.

Results from this study do confirm that lighter albedo and some GREIs represented in this area do demonstrate increased cooling potential as described by other researchers (Santamouris, et.al. 2017). Reflective materials can increase surface albedo which can enhance heat dissipation, resulting in both lower surface temperature and ambient temperature (Qi, et. al. 2019). Evidence from this study indicates that different roofing materials can store, discharge, or transfer heat energy potentially offering passive ways to mitigate UHIs in urbanized areas. Remote sensing technology has become advanced enough to determine temperature differences between different materials and textures, allowing researchers more opportunities to measure and monitor changes in UHIs.

While the research presented in this study supports the theories and findings from other researchers, more research is needed to fully comprehend how large commercial structures affect UHIs in urbanized areas. While remote sensing data collected from LandSat 8 is beneficial, it is also limited because of scale and frequency. The helio-synchronous orbit of the LandSat 8 satellite provides both limited opportunities and information on specific study areas. Also given the size of the area covered by a single LandSat 8 image, the 100 by 100-meter thermal pixel size

makes studying smaller structures difficult, as its limited analysis of this study only very large buildings (over 100,000 square feet/10,000 square meters). While this study attempted to capture discrete temperatures from the approximate center of study sites, aggregate temperature readings were undoubtedly influenced by adjacent pixels, which represented parking lots and vegetation that surround the buildings.

The frequency (approximately two potential images every two weeks for the study site over one year) in conjunction with usable days (less than 25% cloud cover) also limited the scope of this research study. Access to on-site temperature recordings or overnight rooftop temperatures would have enhanced this study with more statistical data, offering more insight into both daily and weekly temperature variations. Several of the rooftops in this study also had large air conditioning units installed on their rooftops, which also could affect rooftop surface temperature reading from the heat generated while the units are in operation. Functionality (retail/commercial vs industrial/warehouse) may also influence these rooftop temperatures, as insulation, internal temperatures, and ventilation are different for each respective site.

Additionally, the focus of this study was only on very large commercial, retail, and warehouse facilities in western Guilford County. There are several large industrial/manufacturing centers as well as other smaller commercial, retail, and warehouse facilities that could be explored in future research, to investigate how their rooftop temperatures and roofing materials compare or interact with the ones in this study. As this area continues to experience an increase in urban development, the promotion of mixed-use zoning (combinations of residential, industrial, and commercial zoning) will require more research to find better ways to offset potential increases in UHIs.

Nonetheless, this case study offered some potential insight into understanding the effects of different roofing materials and their surface temperatures as they relate to UHIs. Given that a majority of buildings in this study are older (26 years or more) they are quickly approaching a need for roof renovation or replacement. As evidence from this study indicates, increasing the albedo or changing the roofing material on a low-sloped roof could offer a way to help reduce the building's cooling costs in the latter part of its lifespan. While CMRs have traditionally been used for industrial or warehouse buildings, the large commercial retail store, Costco, used in this study indicates that this material could easily be used for large retail buildings. Additionally, the findings from this study also illustrate the overall temperature constancy of lighter albedos, as this group had the least fluctuations and most consistent rooftop temperatures over one year.

Future research can explore study sites from a larger time scale over several years, offering more ways to understand the potential long-term environmental effects related to UHIs. Using the GIS-based estimation method of Lee and French (2009) could also be helpful in forecasting increases in impervious surface developments for western Guilford County, to limited increases in UHIs. Additionally, monitoring GREIs could help ascertain the effectiveness of future construction materials for low-slope roofs of large buildings to help reduce urban temperatures or mitigate the effects of UHIs.

Future studies could also focus on the degradation of albedo over several years as a result of weathering, to see how color changes affect the surface temperature of roofing materials over long periods. As the only study site in this paper with large PV solar panels, DE Solar's combination of an averaged medium albedo and PVC/TPO roofing material is another area for future potential research, and could provide a sound strategy for producing electricity as well as cooling a large facility.

REFERENCES

Akbari, H., Pomerantz, M., Taha, H., and Lawrence Berkeley National Lab. (1998). Cool surfaces and shade trees to reduce energy use and improve air quality in urban areas. *Solar Energy*, 70(3).

Akbari, H., Berdahl, P., Levinson, R., Wiel, S., Miller, B., & Desjarlais, A. (2006). *Cool color roofing materials*. CA: Lawrence Berkeley National Laboratory Berkeley.

Assessing the impacts of land-use/land-cover change on the development of urban heat island effects. (2020). *Environment, Development and Sustainability*, 22(8), 7547–7557. https://doi.org/10.1007/s10668-019-00535-w

Atkinsin, B. W. (2003). Numerical Modelling of Urban Heat-Island Intensity. *Boundary-Layer Meteorology*, 109, 285-310.

Baghdadi, N., and Zribi, M. (2016). *Land Surface Remote Sensing in Urban and Coastal Areas*. Remote Sensing Observations of Continental Surfaces Set. London: ISTE.

Baik, J., Kim, Y., Kim, J., and Han, J. (2007). Effects of boundary-layer stability on urban heat island-induced circulation. *Theoretical and Applied Climatology*, 89, 73-81.

Barron-Gafford, G., Minor, R., Allen, N., Cronin, A., Brooks, A., and Pavao-Zuckerman, M. (2016). "The Photovoltaic Heat Island Effect: Larger Solar Power Plants Increase Local Temperatures." *Scientific Reports* 6 (1). https://doi.org/10.1038/srep35070.

Belongie, S., Malik, J. and Puzicha, J. (2002). "Shape matching and object recognition using shape contexts". *The IEEE Transactions on Pattern Analysis and Machine Intelligence*, Vol. 24 No. 4, pp. 509-522.

Braga, A., Zanobetti, A. and Schwartz J. (2002). The effects of weather on respiratory and cardiovascular deaths in 12 US cities. *Environmental Health Perspectives*, 110(9), 859.

Caldwell, C. 1798. *A Semi-Annual Oration, on the Origin of Pestilential Diseases*. Philadelphia: Thomas and Samuel F. Bradford.

Caldwell, C. 1801. A physical sketch of the city of Philadelphia, interspersed with general remarks applicable to all large and populous cities. *In Medical and Physical Memoirs, C. Caldwell*, 1-71. Philadelphia: Thomas and William Bradford.

Casini, M. (2016). *Smart Buildings : Advanced Materials and Nanotechnology to Improve Energy-Efficiency and Environmental Performance*. Woodhead Publishing Series in Civil and Structural Engineering, Number 69. Duxford, UK: Woodhead Publishing

Chen, J., Chu, R., Wang, H., Zhang, L., Chen, X., and Du, Y. (2019). Alleviating urban heat island effect using high-conductivity permeable concrete pavement. *Journal of Cleaner Production*, 237. https://doi.org/10.1016/j.jclepro.2019.117722

Comrie, A. C. (2000). Mapping a wind-modified urban heat island in Tucson, Arizona (with comments on integrating research and undergraduate learning). *Bulletin of the American Meteorological Society*, 81(10), 2417–2431.

Corumluoglu, O., and Asri, I. (2015). "The Effect of Urban Heat Island on Izmir's City Ecosystem and Climate." *Environmental Science and Pollution Research* 22 (5): 3202–11. https://doi.org/10.1007/s11356-014-2874-z.

Cullen, W. C. (1963). "Solar Heating, Radiative Cooling, and Thermal Movement - Their Effects on Built-up Roofing", National Bureau of Standards, Technical Note 231, 1-33.

Debbage, N., and Shepherd, J. M. (2015). "The Urban Heat Island Effect and City Contiguity." *Computers, Environment and Urban Systems* 54: 181–94. https://doi.org/10.1016/j.compenvurbsys.2015.08.002.

Deilami, K., and Kamruzzaman, M. (2017). Modeling the urban heat island effect of smart growth policy scenarios in Brisbane. *Land Use Policy*, 64, 38–55. https://doi.org/10.1016/j.landusepol.2017.02.027

Easterling, D. R., Horton, B., Jones, P. D., Peterson, T. C., Karl, T. R., Parker, D. E., Folland, C. K. (1997). Maximum and minimum temperature trends for the globe. *SCIENCE,* 277, 364-367.

Echevarria Icaza, L, and F.D van der Hoeven. (2017). "Regionalist Principles to Reduce the Urban Heat Island Effect." *Sustainability* 9 (5).

Enríquez E, Fuertes, V., Cabrera, M. J., Seores, J., Muñoz D, and Fernández JF. (2017). New strategy to mitigate urban heat island effect: energy saving by combining high albedo and low thermal diffusivity in glass ceramic materials. *Solar Energy*, 149, 114–114.

Gartland, L. (2008). *Heat islands : understanding and mitigating heat in urban areas* (1st ed.). Earthscan.

"Green Roofs and the Urban Heat Island Effect." (2009). *Buildings* 103 (7): 45–48.

"Green Roof Systems Gaining in Popularity: Energy Saving and Reducing the ``Urban Heat Island" Effect Are Gains from Green Roofs. Dow Describes the Ease of Using Its Verdiseal Pu Membrane in This Technology." (2010). *Urethanes Technology International* 27 (1): 18–21.

Han, J., and Baik, J. (2008). A Theoretical and Numerical Study of Urban Heat Island-Induced Circulation and Convection. *Journal of Atmospheric Sciences*, June, 1859-1877.

He, Z., Tan, T. and Sun, Z. (2009). "Topology modeling for Adaboost-cascade based object detection". *Pattern Recognition Letters*, Vol. 31 No. 1, pp. 912-919

He, B.-J. (2018). Potentials of meteorological characteristics and synoptic conditions to mitigate urban heat island effects. *Urban Climate*, 24, 26–33. https://doi.org/10.1016/j.uclim.2018.01.004

Howard, L (1833). *Climate of London Deduced from Meteorological Observations*. Harvey and Darton, London (3rd Ed.)

Imhoff, M., Zhang. P, Wolfe, R., and Bounoua, L. (2010). "Remote Sensing of the Urban Heat Island Effect Across Biomes in the Continental Usa." *Remote Sensing of Environment* 114 (3): 504–13. https://doi.org/10.1016/j.rse.2009.10.008.

Khaikine, M. N., Kuznetsova, I. N., Kadygrov, E. N., and Miller, E. A. (2006). Investigation of temporal-spatial parameters of an urban heat island on the basis of passive microwave remote sensing. *Theoretical and Applied Climatology*, 84, 161-169.

Kim, H., Gu, D., and Kim, H. Y. (2018). Effects of urban heat island mitigation in various climate zones in the United States. *Sustainable Cities and Society*, 41, 841–852. https://doi.org/10.1016/j.scs.2018.06.021

Kim, S. (2012). "Robust corner detection by image-based direct curvature field estimation for mobile robot navigation". *International journal on advanced Robotic Systems*, Vol. 9 No. 187, pp. 1-12.

Konasova S, and 17th International Multidisciplinary Scientific Geoconference, SGEM 2017 17 2017 11 27 - 2017 11 29. (2017). "The Role of Green Roofs to Mitigate Urban Heat Island Effect." *International Multidisciplinary Scientific Geoconference Surveying Geology and Mining Ecology Management, Sgem* 17 (63): 1047–54. https://doi.org/10.5593/sgem2017H/63/S27.130.

Koomen, E. and Diogo, V. (2017). "Assessing Potential Future Urban Heat Island Patterns Following Climate Scenarios, Socio-Economic Developments and Spatial Planning Strategies." *Mitigation and Adaptation Strategies for Global Change: An International Journal Devoted to Scientific, Engineering, Socio-Economic and Policy Responses to Environmental Change* 22 (2): 287–306. https://doi.org/10.1007/s11027-015-9646-z.

Lai, L. and Chaeng W. (2010) Urban head island and air pollution-an emerging role for hospital respiratory admissions in an urban area. *Journal of Environmental Health*, 72(6), 32.

Liang, S. 2000. "Narrowband to broadband conversions of land surface albedo I algorithms." *Remote Sensing of Environment* 76, 213-238.

Lee, H.-Y. (1993). An application of NOAA AVHRR thermal data to the study of urban heat islands. Atmospheric Environment. Part B, *Urban Atmosphere*, 27(1), 1–13. https://doi.org/10.1016/0957-1272(93)90041-4

Lee, S., and French, S. P. (2009). Regional impervious surface estimation: An urban heat island application. *Journal of Environmental Planning and Management*, 52(4), 477-496.

Liu, N., and Morawska, L. (2020). Modeling the urban heat island mitigation effect of cool coatings in realistic urban morphology. *Journal of Cleaner Production*, 264. https://doi.org/10.1016/j.jclepro.2020.121560

Liu, Y., Li, Q., Yang, L., Mu, K., Zhang, M., and Liu, J. (2020). Urban heat island effects of various urban morphologies under regional climate conditions. *Science of the Total Environment*, 743. https://doi.org/10.1016/j.scitotenv.2020.140589

Lo, C. P., Quattrochi, D.A., and Luvall, J.C. (1997). Application of high-resolution thermal infrared remote sensing and GIS to assess the urban heat island effect. *International Journal of Remote Sensing*, 18(2), 287–304.

Mastrangelo, G. Fedeli, U. Visentin, C. Milan, G., Fadda, E., and Spolaore, P. (2007). Pattern and determinants of hospitalization during heat waves: An ecologic study. *BMC Public Health*, 7 (1), 1.

Memon, R. A., Leung, D. Y., and Liu, C. (2009). An investigation of urban heat island intensity (UHI) as an indicator of urban heating. *Atmospheric Research*, 94, 491-500.

Meng, H., Peng, C., and Xin, H. (2018). Study of the cooling effects of urban green space in Harbin in terms of reducing the heat island effect. *Sustainability*, 10(4). https://doi.org/10.3390/su10041101

Meyer, W. B. (1991). Urban heat island and urban health: early American perspectives. *Professional Geographer*, 43(1), 38–38.

Michelsen, T. (1998). A look ahead: Cooling urban heat islands. *RSI: Roofing, Siding, Insulation*, 75(5), 26.

Mitchell, J. M. (1961). The temperature of cities. *Weatherwise*, 14(6), 224–258. https://doi.org/10.1080/00431672.1961.9930028

Nakayama, T., and Fujita, T. (2010). Cooling effect of water-holding pavements made of new materials on water and heat budgets in urban areas. *Landscape and Urban Planning*, 57-67.

Nichol, J.E., and Wong, M.S. (2005). Modeling urban environment quality in a tropical city. *Landscape and Urban Planning*, 73(1), 49-58.

Nichol, J. E., Fung, W. Y., Lam, K., and Wong, M. S. (2009). Urban heat island diagnosis using ASTER satellite images and 'in situ' air temperature. *Atmospheric Research*, 94, 276-284.

Niino, H., Mori, A., Satomura, T., and Akiba, S. (2006). Flow Regimes of Nonlinear Heat Island Circulation. *Journal of the Atmospheric Sciences*, 63, 1538-1547.

Oke, T. R. (1982). The energetic basis of the urban heat island. *Quarterly Journal of the Royal Meteorological Society*, 108(455), 1–24.

Oke, T. R., Mills, G., Christen, A., and Voogt, J.A., (2017) *Urban Climates*. Cambridge University Press.

Parker, D. E. (2010). "Urban Heat Island Effects on Estimates of Observed Climate Change." *Wiley Interdisciplinary Reviews: Climate Change* 1 (1): 123–33. https://doi.org/10.1002/wcc.21.

Prasad, M., Zisserman, A., Fitzgibbon, A., Kumar, M.P., and Torr, P.H.S. (2006). "Learning class-specific edges for object detection and segmentation". *Lecture Notes in Computer Science*, Vol. 4338, pp. 94-105.

Qi, J.D., He, B.J., Wang, M., Zhu, J., and Fu, W.C. (2019). Do grey infrastructures always elevate urban temperature? no, utilizing grey infrastructures to mitigate urban heat island effects. *Sustainable Cities and Socie*ty, 46, 101392–101392. https://doi.org/10.1016/j.scs.2018.12.020

Qiu, G. Y., Zou, Z., Li, X., Li, H., Guo, Q., Yan, C., and Tan, S. (2017). Experimental studies on the effects of green space and evapotranspiration on urban heat island in a subtropical megacity in China. *Habitat International*, 68, 30–42. https://doi.org/10.1016/j.habitatint.2017.07.009

Quattrochi D.A., and Luvall J.C. (1999) Thermal infrared remote sensing for analysis of landscape ecological processes: methods and applications. *Landscape Ecology* 14(6):577–598

Rajasekar, U., and Weng, Q. (2009). Urban heat island monitoring and analysis using a non-parametric model: a case study of Indianapolis. *Isprs Journal of Photogrammetry and Remote Sensing*, 64(1), 86–96. https://doi.org/10.1016/j.isprsjprs.2008.05.002

Reid, R. (2000). *Roofing & Cladding Systems : A Guide for Facility Managers*. Lilburn, Ga: Fairmont Press. http://search.ebscohost.com.proxy078.nclive.org/login.aspx?direct=true&db=nlebk&AN=38935&site=ehost-live.

Renou, E. (1862). 'Differences de temperature entre Paris et Choisy-le-Roi". *Annuaire Societe Meteorlogique de France* 10: 105-109.

Riedmiller, B.M., Springenberg, T.J., Wülfing, J. and Martin, A. (2012). "A learned feature descriptor for object recognition in RGB-D data". *IEEE International Conference on Robotics and Automation* (ICRA), Breisgau, pp. 1298-1303.

Rossiter, W. and Mathey R. (1976) “Effects of Insulation on the Surface Temperature of Roof Membranes”. Center for Building Technology: Institute for Applied Technology. *National Bureau of Standards*, NBSIR 76-987, 1-15.

Rothwell, C., Mundy, J., and Hoffman, B. (1996). “Representing objects using topology”. *Lecture Notes in Computer Science*, Vol. 1144, pp. 79-108.

Salamanca, F., Georgescu, M., Mahalov, A., Moustaoui, M., & Martilli, A. (2016). Citywide impacts of cool roof and rooftop solar photovoltaic deployment on near surface air temperature and cooling energy demand. *Boundary-layer Meteorology*, 161(1), 203–221.

Santamouris, M., Synnefa, A., and Karlessi, T. (2011). Using advanced cooling materials in urban built environment to mitigate heat islands and improve thermal comfort conditions. *Solar Energy*, 85(12). 3085-3102.

Santamouris, M., Ding, L., Fiorito, F., Oldfield, P., Osmond, P., Paolini, R., Prasad, D., and Synnefa, A. (2017). Passive and active cooling for the outdoor built environment – analysis and assessment of the cooling potential of mitigation technologies using performance data from 220 large scale projects. *Solar Energy*, 154, 14–33. https://doi.org/10.1016/j.solener.2016.12.006

Schatz, J., and Kucharik, C. (2014). “Seasonality of the Urban Heat Island Effect in Madison, Wisconsin.” *Journal of Applied Meteorology and Climatology* 53 (10): 2371–86.

Siddula, M., Fei, D., Yanfang, Y., and Jianping, F. (2016). “Classifying construction site photos for roof detection.” *Construction Innovation* 16, (3): 368-389, https://login.libproxy.uncg.edu/login?url=https://www.proquest.com/scholarly-journals/classifying-construction-site-photos-roof/docview/1826443362/se-2?accountid=14604.

Silva H., Phelan P., and Golden J. (2010). “Modeling Effects of Urban Heat Island Mitigation Strategies on Heat-Related Morbidity: A Case Study for Phoenix, Arizona, Usa.” *International Journal of Biometeorology* 54 (1): 13–22. https://doi.org/10.1007/s00484-009-0247-y.

Smith, C., and Levermore, G. (2008). Designing urban spaces and buildings to improve sustainability and quality of life in a warmer world. *Energy Policy*, 4558-4562.

Smith, R.B. (2010). “The heat budget of the earth’s surface deduced from space”. Yale University Center for Earth Observation: New Haven, CT.

Stewart, I. D., and Mills, G. M. (2021). *The Urban Heat Island: a guidebook*. Elsevier.

Stone, B., and Norman, J. M. (2006). Land use planning and surface heat island formation: A parcel-based radiation flux approach. *Atmospheric Environment*, 3561-3573.

Streutker, D. R. (2002). A remote sensing study of the urban heat island of Houston, Texas. *International Journal of Remote Sensing*, 23(13), 2595–2608.

Sun, R., and Chen, L. (2017). Effects of green space dynamics on urban heat islands: mitigation and diversification. *Ecosystem Services*, 23(C), 38–46.

Synnefa, A., Dandou, A., Santamouris, M., and Tombrou, M. (2008). On the Use of Cool Materials as a Heat Island Mitigation Strategy. *Journal of Applied Meteorology & Climatology*, 2846-2856.

Tsai, F.C. (2007). "Image mining by spectral features: a case study of scenery image classification". *Expert Systems with Applications*, Vol. 32 No. 1, pp. 135-142.

Theeuwes, N.E, Steeneveld, G. J., Ronda, R.J., and Holtslag, A. A. M. (2017). "A Diagnostic Equation for the Daily Maximum Urban Heat Island Effect for Cities in Northwestern Europe." *International Journal of Climatology* 37 (1): 443–54.

Urban heat island effects depend on city's layout. (2018). *Laboratory Equipment*, N/A.

U.S. Energy Information Administration - EIA - independent statistics and analysis. North Carolina - State Energy Profile Overview - U.S. Energy Information Administration (EIA). (n.d.). Retrieved March 10, 2022, from https://www.eia.gov/state/?sid=NC

Voogt, J. A. (2000). Image representations of complete urban surface temperatures. *Geocarto International*, 15(3), 21–32.

Voogt, J. A. and Oke, T. R. (2003). Thermal remote sensing of urban climates. *Remote Sensing of Environment*, 86(3), 370–384. https://doi.org/10.1016/S0034-4257(03)00079-8

Xu, S. (2009). "An Approach to Analyzing the Intensity of the Daytime Surface Urban Heat Island Effect at a Local Scale." *Environmental Monitoring and Assessment : An International Journal Devoted to Progress in the Use of Monitoring Data in Assessing Environmental Risks to Man and the Environment* 151 (1-4): 289–300. https://doi.org/10.1007/s10661-008-0270-1.

Wang, W., Kai L., Rong T., and Shudong, W. (2019). "Remote Sensing Image-Based Analysis of the Urban Heat Island Effect in Shenzhen, China." *Physics and Chemistry of the Earth* 110: 168–75. https://doi.org/10.1016/j.pce.2019.01.002.

Weng Q., Lu D., and Schubring J. (2004) Estimation of land surface temperature vegetation abundance relationship for urban heat island studies. *Remote Sensing Environment* 89(4):467–483

Yang, P., Zi-Niu X., and Meng-Shu, Y. (2016). “Cooling Effect of Urban Parks and Their Relationship with Urban Heat Islands.” *Atmospheric and Oceanic Science Letters* 9 (4): 298–305. https://doi.org/10.1080/16742834.2016.1191316.

Yang, F., Lau, S. S., and Qian, F. (2011). Urban design to lower summertime outdoor temperatures: An empirical study on high-rise housing in Shanghai. *Building and Environment*, 769-785.

Yang, Z., Hurd, J., and Kao, W. (2020). Using Landsat 8 data to compare percent impervious surface area and normalized difference vegetation index as indicators of urban heat island effects in Connecticut. *Environmental Earth Sciences*, 79(18). https://doi.org/10.1007/s12665-020-09159-0

Yang, J., Yichen W., Chunliang X., Xiangming X., Jianhong X., and Cui, J. (2020). “Optimizing Local Climate Zones to Mitigate Urban Heat Island Effect in Human Settlements.” *Journal of Cleaner Production* 275. https://doi.org/10.1016/j.jclepro.2020.123767.

Young-bae, S. (2005). Influence of new town development on the urban heat island – The case of the Bundang area. *Journal of Environmental Sciences*, 641-645.

Zhang, H., Gao, W., Chen, X. and Zhao, D. (2006). “Object detection using spatial histogram features”. *Image and Vision Computing*, Vol. 24 No. 4, pp. 327-341.

Zeman, F. (2012). *Metropolitan Sustainability: Understanding and Improving the Urban Environment*. Woodhead Publishing Series in Energy, No. 34. Cambridge, UK: Woodhead Pub.

APPENDIX A: RECORDED TEMPERATURE TABLES

Table 9: Recorded Temperatures in Degrees Fahrenheit °F for the city of Greensboro and study sites with dark albedo

Date	GSB0 City Temp	USPS-DC	GAB	FEDEX	GIL	AP1	GBF	FASTD	USPS-NDC
25-Dec-19	56	67	53	17	39	48	53	53	46
17-Jan-20	44	55	46	12	30	37	48	46	39
26-Jan-20	50	64	52	14	32	37	50	50	43
2-Feb-20	61	68	52	16	37	43	52	50	46
27-Feb-20	47	68	55	12	32	43	52	50	46
6-Apr-20	80	88	80	52	59	73	79	75	75
22-Apr-20	68	99	82	43	64	71	71	79	75
24-May-20	85	91	82	64	75	79	79	79	80
2-Jun-20	82	99	86	64	75	80	86	95	80
4-Jul-20	91	111	95	77	85	91	95	84	93
11-Jul-20	89	115	93	68	82	89	91	93	91
20-Jul-20	94	108	93	77	84	88	91	93	89
27-Jul-20	92	104	86	71	82	86	89	89	86
6-Sep-20	80	111	79	62	80	64	91	91	86
22-Sep-20	70	106	91	44	79	86	80	82	75
8-Oct-20	81	100	82	59	64	71	84	82	80
24-Oct-20	80	90	86	59	73	79	77	79	75
9-Nov-20	75	91	75	50	64	66	75	75	70
16-Nov-20	60	77	75	53	64	66	79	75	55
2-Dec-20	52	64	66	28	46	52	61	61	41
11-Dec-20	62	75	50	28	33	51	61	57	52
18-Dec-20	44	55	59	10	46	52	44	43	39
27-Dec-20	49	54	32	8	32	30	28	26	17

Table 10: Recorded Temperatures in Degrees Fahrenheit °F for the city of Greensboro and study sites with medium albedo

Date	GSB0 City Temp	COS	DE	LOW	HTNS	CME	AP2	CAM
25-Dec-19	56	46	52	50	50	12	50	52
17-Jan-20	44	41	41	43	41	12	44	44
26-Jan-20	50	43	46	44	43	16	46	46
2-Feb-20	61	37	50	48	48	21	52	50
27-Feb-20	47	32	48	48	44	10	50	50
6-Apr-20	80	71	70	73	73	55	73	80
22-Apr-20	68	71	75	75	75	34	73	71
24-May-20	85	77	80	79	77	62	77	75
2-Jun-20	82	79	82	80	59	61	82	82
4-Jul-20	91	89	95	89	86	75	91	91
11-Jul-20	89	88	91	89	97	70	88	91
20-Jul-20	94	86	89	88	88	73	88	84
27-Jul-20	92	75	88	75	88	73	86	82
6-Sep-20	80	82	88	82	88	59	86	88
22-Sep-20	70	70	77	87	95	46	75	74
8-Oct-20	81	73	80	75	75	55	79	80
24-Oct-20	80	70	75	79	88	57	75	75
9-Nov-20	75	66	73	71	79	59	71	73
16-Nov-20	60	50	61	71	79	52	73	79
2-Dec-20	52	35	46	59	61	35	57	46
11-Dec-20	62	48	57	44	48	25	57	57
18-Dec-20	44	32	39	55	62	10	43	37
27-Dec-20	49	21	37	42	37	21	37	39

Table 11: Recorded Temperatures in Degrees Fahrenheit °F for the city of Greensboro and study sites with light albedo

Date	GSB0 City Temp	HTSS	HD	SC	AH	WAL	UNI	FASTF	POLO	BER	NFI	AMA
25-Dec-19	56	52	52	53	52	53	50	50	50	50	50	50
17-Jan-20	44	43	44	52	44	52	44	41	44	43	46	44
26-Jan-20	50	52	48	52	50	52	48	46	48	46	48	46
2-Feb-20	61	52	52	48	52	48	50	52	52	50	48	50
27-Feb-20	47	53	52	44	52	44	48	50	50	48	48	48
6-Apr-20	80	73	77	77	75	77	71	80	79	73	73	73
22-Apr-20	68	84	80	77	79	77	73	80	75	79	73	75
24-May-20	85	84	80	80	79	80	77	82	80	77	77	80
2-Jun-20	82	82	84	86	84	86	84	88	85	80	82	84
4-Jul-20	91	93	95	95	95	95	91	91	84	91	91	93
11-Jul-20	89	91	93	93	91	93	93	93	93	89	91	88
20-Jul-20	94	91	89	89	89	89	89	91	91	88	89	89
27-Jul-20	92	86	86	84	86	84	88	88	88	84	86	86
6-Sep-20	80	86	75	89	77	89	86	86	89	73	86	86
22-Sep-20	70	93	89	79	89	79	77	75	80	88	77	79
8-Oct-20	81	84	80	82	79	82	82	79	82	79	79	79
24-Oct-20	80	84	82	77	82	77	75	75	77	82	75	75
9-Nov-20	75	75	73	73	73	73	86	70	73	71	73	71
16-Nov-20	60	75	73	61	73	61	71	80	79	71	73	77
2-Dec-20	52	64	61	57	62	57	44	55	59	61	57	57
11-Dec-20	62	50	46	57	48	57	55	55	59	46	57	57
18-Dec-20	44	59	57	35	57	35	43	35	35	55	43	41
27-Dec-20	49	37	32	30	35	30	32	61	44	44	26	37